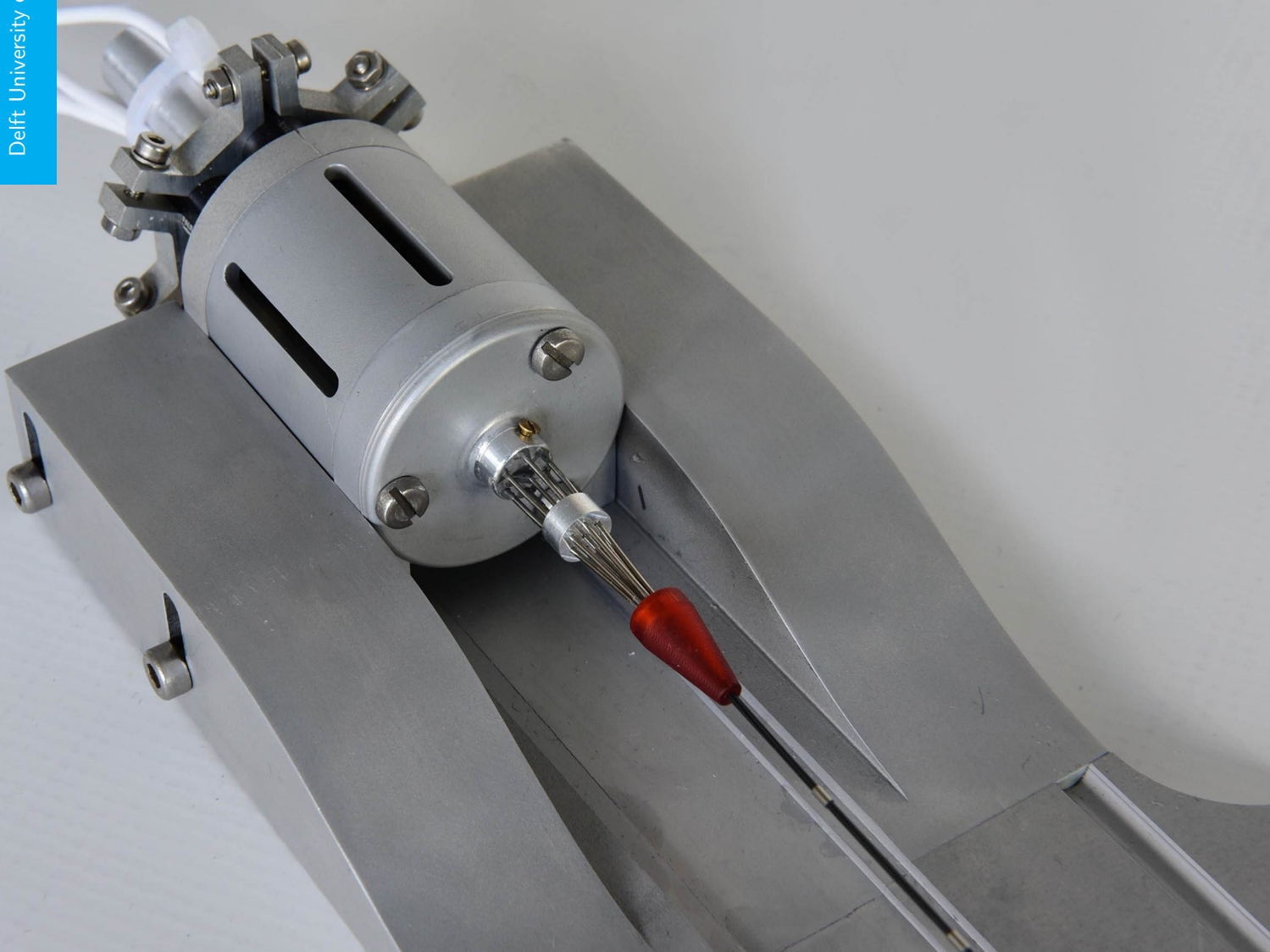


From the Wasp Ovipositor to a 3D Steerable Needle for Solid-Tissue Interventions

A Design and Experimental Approach

Tim P. Pusch

Delft University of Technology



FROM THE WASP OVIPOSITOR TO A 3D STEERABLE NEEDLE FOR SOLID-TISSUE INTERVENTIONS

A DESIGN AND EXPERIMENTAL APPROACH

by

Tim P. Pusch

in partial fulfillment of the requirements for the degree of

Master of Science
in Mechanical Engineering

at the Delft University of Technology,
to be defended publicly on Thursday May 19, 2016 at 10:00 AM.

Supervisors:	M. Scali	
	Dr. D. Dodou	
	Prof. dr. ir. P. Breedveld	
Thesis committee:	Prof. dr. ir. P. Breedveld,	TU Delft
	Dr. D. Dodou,	TU Delft
	Dr. ir. D. H. Plettenburg,	TU Delft
	Dr. ir. M. Langelaar,	TU Delft
	M. Scali,	TU Delft

An electronic version of this thesis is available at <http://repository.tudelft.nl/>.

CONTENTS

1	Introduction	1
2	Scientific Paper	3
2.1	Introduction	5
2.1.1	Motivation for Needle Steering.	5
2.1.2	State-of-the-Art in Steerable Needle Designs.	5
2.1.3	Biological Inspiration for Steerable Needle Design.	5
2.1.4	Aim of this Work	6
2.2	Design of the Needle	6
2.2.1	Design Objectives	6
2.2.2	Conceptual Design.	6
2.2.3	Final Design	7
2.2.4	Forward Motion and Steering of the Needle	8
2.3	Design of the Actuation Unit	9
2.3.1	Design Considerations	9
2.3.2	Conceptual Design Process	10
2.3.3	Description of the Final Design	12
2.4	Experimental Validation	13
2.4.1	Dependent and Independent Variables	13
2.4.2	Hypotheses	13
2.4.3	Experimental Setup	13
2.4.4	Experimental Design.	14
2.4.5	Gelatin Preparation	15
2.4.6	Experimental Procedure	15
2.4.7	Data Analysis	15
2.5	Results	16
2.5.1	Experiment 1.	16
2.5.2	Experiment 2.	16
2.6	Discussion	16
2.6.1	Steerable Needle Concept	16
2.6.2	Interpretation of Results	16
2.6.3	Limitations.	18
2.6.4	Future Work	18
2.7	Conclusion	19
	References	19
A	Engineering Drawings	23
B	Arduino Code	39
B.1	Main sketch.	40
B.2	moveMotor function	45
C	Experiments	47
C.1	Experiment 1	47
C.2	Experiment 2	48
D	MATLAB Code	49
D.1	Experiment 1 (slip analysis)	49
D.2	Experiment 2 (steering analysis)	55

1

INTRODUCTION

This report discusses the design and experimental evaluation process of a novel steerable needle inspired by the egg-laying channel ('ovipositor') of parasitic wasps. The main contribution of this work is summarized in chapter 2, written in the style of a scientific paper. Here, the motivation for this study is outlined followed by the design and experimental procedure, the discussion and interpretation of the results and the conclusions that could be drawn. Several appendices are provided to give the reader deeper insight into the design (appendix A & B) and methods (appendix C & D) sections of the scientific paper. Specifically, appendix A shows the engineering drawings of the mechatronic needle prototype that was developed and built. Appendix B outlines the software and control logic responsible for actuating the needle prototype in the desired fashion. In appendix C more details on the experiments performed in this study are provided. Lastly, appendix D contains the code used for the analysis of the data gathered in the experiments as well as instructions on how to use this code.

2

SCIENTIFIC PAPER

From the Wasp Ovipositor to a 3D Steerable Needle for Solid-Tissue Interventions - A Design and Experimental Approach

Tim P. Pusch

Abstract—In many percutaneous interventions, such as biopsies and brachytherapy, accuracy in reaching a specific target inside the human body is necessary for the success of the procedure. Maneuvering to the target site is challenging, particularly if sensitive structures such as blood vessels have to be avoided. For maneuvering along a curved trajectory, flexible steerable needles have been introduced. However, since needles generally require a push force to be advanced into the tissue, the flexible nature of steerable needles makes them prone to buckling. Moreover, many steerable needles require rotation for maneuvering in a 3D space, causing needle twisting which makes accurate control of the needle challenging. In this study, a novel approach for the design of a flexible needle inspired by the egg-laying channel ('ovipositor') of parasitic wasps is proposed which addresses the aforementioned steering and buckling challenges while being small enough to be used in biopsy and brachytherapy procedures. This approach has led to the development of a six-segmented needle prototype designed to be both steerable in 3D without the need for rotation and devoid of the need for an axial push force for insertion into tissue thereby eliminating the risk of needle buckling. Experimental validation of our $\varnothing 1.2$ mm needle prototype in porcine gelatin specimen showed promising results, with steering curvatures of 0.018 1/cm achievable; yet further refinement of the design and experimental setup is necessary for a conclusive experimental assessment of the needle prototype.

Keywords—Steerable needles, medical needles, solid-tissue, biologically inspired design.

I. INTRODUCTION

A. Motivation for Needle Steering

In many types of percutaneous procedures such as internal radiation therapy (brachytherapy), biopsies, and localized drug delivery, medical needles are used to reach the target site. Accuracy in maneuvering the needle toward the target is vital for the success of these procedures, as placement errors can lead to a false diagnosis in biopsies [1], [2] and poor dosimetry in brachytherapy [3], and can cause neurological complications in peripheral anesthesia [4]. Furthermore, if the needle is misplaced, it should be withdrawn and reinserted, a corrective action that not only elongates the procedure but can also cause post-operative discomfort to the patient due to iatrogenic tissue trauma [5].

Deviation from the pre-operatively planned trajectory during needle insertion has been attributed, among others, to undesired needle redirection inside the tissue [3], displacement of

the target due to tissue deformation caused by the needle insertion [6] and human error [7], [8]. In such cases, intra-operative adjustment of the needle path is necessary. Conventional rigid straight needles, however, only allow for marginal intra-operative path adjustments. Moreover, rigid straight needles are inadequate for procedures in which a curved trajectory is desired [9]. Flexible steerable needles have the potential to help surgeons reach a target with greater accuracy than when using straight needles, as well as enable them to reach targets that are inaccessible to straight needles.

B. State-of-the-Art in Steerable Needle Designs

Several steerable needle designs and mechanisms have been described in the literature [10]–[13]. In some of the proposed mechanisms deflection (i.e. steering) of the needle is enabled due to the pre-defined needle shape (e.g., bevel-tip needles [14], [15] and needles with a pre-curvature [16], [17]), whereas in other needles steering is realized on-demand by means of actuated elements (e.g., tendon-actuated needles [18], [19]).

A main drawback of flexible needles is that they are prone to buckling, particularly when they are advanced deep inside the body [20]. Moreover, many of the proposed steerable needle designs are limited to 2D steering (e.g., bevel-tip needles), which means that they require axial rotation to be maneuvered in a 3D space. Rotating a needle when inside a tissue may cause the needle to twist due to friction forces between the tissue and the needle shaft. Since the needle trajectory depends on the axial orientation of the needle tip, an angular lag between needle tip and needle base caused by this twist poses a challenge to the control of the needle path [21], [22].

C. Biological Inspiration for Steerable Needle Design

Percutaneous needle interventions bear a similarity to the egg-laying process of female parasitic wasps of the Hymenoptera family in that a long and slender device is used to maneuver through an inhomogeneous substrate (i.e., wood or fruits in the case of the wasp vs. tissue in the case of needles) in order to accurately reach a specific target (i.e., host larva vs. target tissue). The marvel of the egg-laying channel ('ovipositor') used by the wasp for this task lies in the anatomy and steering mechanism of the ovipositor which allow it to be thin (i.e., aspect ratio of more than 200 in some species [24]), yet not prone to buckling and steerable in a 3D space.

The wasp ovipositor consists of several dovetail-interlocked segments ('valves') that can slide relative to one another ([23],

Tim P. Pusch is with the Department of Biomechanical Engineering, Delft University of Technology, Delft, The Netherlands. E-mail: pusch.tim@gmail.com.

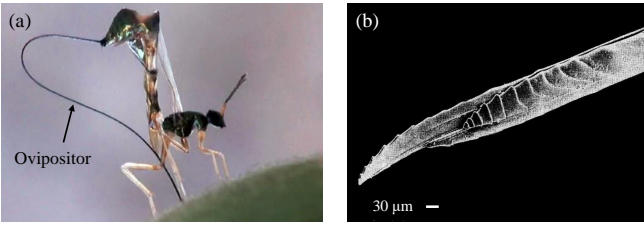


Fig. 1: (a) Wasp inserting ovipositor into a fig, modified from [48]. (b) Scanning electron microscope image of the front part of the wasp ovipositor (modified from [24]).

Figure 1). In order to advance the ovipositor through the substrate, the ovipositor segments are pushed forward in an alternating fashion: one segment is advanced at a time, while the remaining two (or, in some species, more) segments are pulled back, anchoring in the substrate by means of backward-facing hooks on the valve surface. The thereby created pre-tension in the ovipositor as well as the static friction between the ovipositor and the substrate compensate the cutting and dynamic friction force of the advancing segment [24], [25]. The wasp uses this push-pull mechanism to prevent buckling of the ovipositor.

The segmented anatomy of the ovipositor also allows steering through the substrate. Several hypotheses regarding the steering mechanism have been proposed [26], [27], according to which steering is achieved by selectively advancing valves to initiate steering in the desired direction.

The advancing and steering mechanism of the wasp ovipositor has inspired the design of devices for planetary drilling [28], bone drilling in hip joint surgery [29] and medical needles and probes [30], [31]. As an example, the 3D steerable probe by Frasson et al. [30] consists of four segments held together by a jigsaw-puzzle interlocking mechanism similar to the one found in the ovipositor. The four segments can slide relative to one another and use serrations on the surface of the segments that compensate the cutting and the dynamic friction force of advancing segments. Moreover, the alternating advancement of the needle segments restricts target movements [32] and tissue strain [33] as compared to pushing all segments simultaneously. Each segment has a beveled tip which enables deflection of the segment when advanced individually. The probe is steered in the desired direction by first advancing one of the needle segments, causing it to deflect in the direction of its bevel. Next, all needle segments are pushed forward simultaneously following the trajectory prescribed by the individually advanced segment. Extensive research has been done on the optimization of the design of this probe (e.g., [34], [35]), modeling and control strategies (e.g., [36], [37]) and experimental testing (e.g., [33], [38]). The thinnest reported prototype of this probe has an outer diameter of 4 mm [32]. Another medical needle inspired by the ovipositor of parasitic wasps was reported by Sprang [31]. This needle consists of four segments with a smooth surface that are pushed forward in an alternating fashion. Compensation of the cutting and the dynamic friction force of an advancing segment is

achieved solely by the difference in contact area between the stationary and advancing segments. The needle is 2 mm in diameter and can follow straight paths.

D. Aim of this Work

This work builds upon existing work in the field of ovipositor-inspired steerable needles and probes and proposes a novel design approach that is particularly useful for the design of needles thin enough to be used in procedures such as brachytherapy and core-needle biopsy (i.e., less than 2 mm). With respect to its functionality, the needle should be able to move forward by means of reciprocating its segments as well as to steer in 3D without the need of axial rotation of the needle. In this paper we first outline the conceptual design process of our steerable needle followed by the development and experimental validation of a needle prototype.

II. DESIGN OF THE NEEDLE

A. Design Objectives

Our objective in this study was to design a research prototype of a multi-segmented needle that advances forward by reciprocally moving its segments in an alternating fashion and that can steer in 3D without axial rotation. In terms of dimensions, we aimed for a needle diameter smaller than 2 mm (approx. 14-gauge) to conform with commonly used needles for core-needle biopsy (14- to 19-gauge, [41]) and brachytherapy (17- to 18-gauge, [42], [43]) procedures.

B. Conceptual Design

1) *Shape of Needle Segments:* The direct technical analogue of the wasp ovipositor valves (Figure 2) is a needle consisting of two or more cylindrical sectors (e.g., halves, thirds, or quarters of a cylinder) aligned along each other in such a way that they form an overall cylindrical shape. Such needle prototypes consisting of two- and four-cylindrical sector segments have been reported in the literature (e.g., [38], [45], [46]). However, manufacturing long and well-aligned sector-shaped needle segments of a size suitable for procedures such as core-needle biopsy and brachytherapy is technically challenging. A way to bypass such manufacturability limitations is by reasoning that the smaller the radius of the cylindrical sector, the closer it can be approximated by a cylinder with a diameter equal to the radius of the cylindrical sector. Following this reasoning, we decided to use off-the-shelf round wires as independently movable segments instead of machined cylindrical sectors. This way, the miniaturization of the needle diameter primarily depends on the availability of small-diameter wires rather than on the manufacturability of cylindrical sectors (Figure 2).

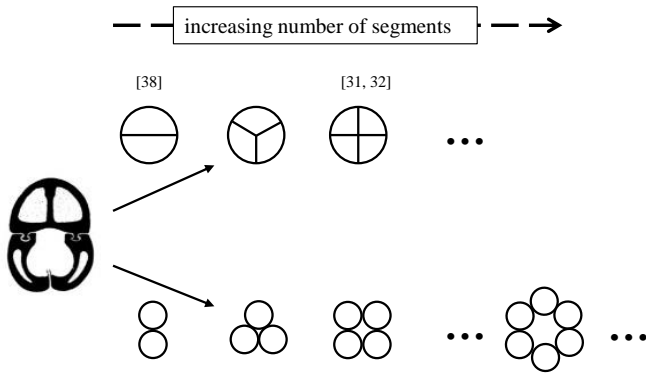


Fig. 2: Figure showing the design evolution of the cross section of our needle from the three-valve ovipositor cross-section on the left-hand side of the figure (modified from [23]) to the six-segmented cross-section of our needle on the bottom right-hand side. The upper branch shows possible needle designs using circular-sector shaped segments, while possible needle designs using round segments, as proposed in this work, are shown in the lower branch. References indicate existing prototypes of a particular needle design.

2) *Number of Needle Segments:* Choosing the number of reciprocally moving segments (in our case: wires) represents an optimization problem between versatility in choosing the steering direction, bending stiffness, overall diameter and slip during forward motion of the needle. Deflection of needles stems from radial asymmetry in the needle shape [10]. In many steerable needle designs this radial asymmetry is achieved by using a bevel-tip, which, when inside a solid substrate (e.g., tissue), causes the needle to deflect as a result of unbalanced forces applied by the tissue on the bevel. The main drawback of a bevel-tip is that it has a preferred predefined orientation and thus its steering capability is limited to 2D steering; as mentioned in the introduction, steering a beveled needle in 3D requires axial rotation

To allow for 3D steering without axial rotation, we make use of the segmented nature of our prototype. Specifically, by selectively advancing one or more segments, radial asymmetry at the tip can be created. The steering direction and the steering angle can be varied by choosing different combinations of segments to protrude and different offsets (see Figures 3 and 6).

From a steerability point-of-view, choosing the number of segments is an optimization problem between the number of possible tip shapes and the bending stiffness of the needle. The number of possible tip shapes that can be created in this way increases exponentially with the number of individually movable segments that are available. On the other hand, the more needle segments, the larger the overall diameter of the needle will be. A larger needle diameter negatively affects steering by increasing the bending stiffness of the needle compared to a needle with fewer needle segments and hence a smaller diameter.

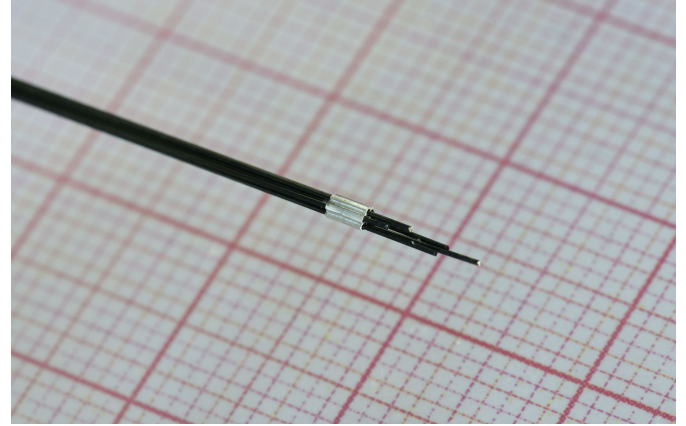


Fig. 3: Close-up photograph of the needle tip showing the NiTi wires and the interlocking ring.

For advancing the needle, choosing the number of segments is an optimization problem between net push force and needle size. Specifically, net push force decreases and can be minimized when the friction of the stationary segments is sufficiently high to compensate for the sum of the dynamic friction and cutting forces of the advancing segment(s). If the necessary force for advancing the segment(s) is not fully compensated, slip between the needle and the substrate occurs, causing a lag between the actual and desired insertion depth of the needle. Therefore, a needle with a high ratio between the number of stationary and moving segments will slip less during forward motion than a needle in which this ratio is low. Consequently, for achieving a high ratio between the number of stationary and moving segments, a needle with a large number of needle segments is advantageous compared to a needle constructed of only a few segments. On the other hand, the larger the number of segments, the larger the total diameter of the needle which may limit its applicability to percutaneous interventions.

In this feasibility study we did not solve the aforementioned optimization problem but rather selected the smallest number of segments that would allow us to study whether forward motion and steering of a needle consisting of cylindrical untreated (i.e., without bevel-tip and microtextured surface) segments is viable. Thus, the rationale behind the selected number of needle segments for our prototype is as follows: to be able to create asymmetry between advancing segments while maintaining a ratio between stationary to moving segments of greater than one, at least five segments are necessary. To allow for steering in two perpendicular planes a symmetric six-wire design was chosen (Figure 2).

C. Final Design

The needle prototype consists of six Nickel Titanium (NiTi) wires (i.e., needle segments) with a diameter of 0.25 mm and a length of 160 mm. The wires can slide along the length of the needle independently from each other and are concentrically

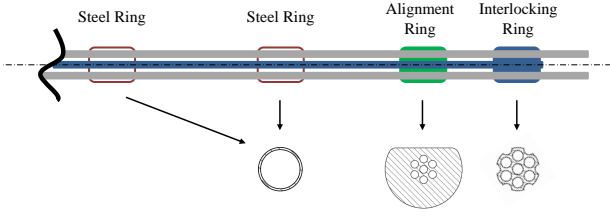


Fig. 4: Schematic drawing of the needle showing the different rings used. Only three of the seven wires and two of the five steel rings are shown.

arranged around a seventh - passive - NiTi wire ($d = 0.25$ mm) at the needle center which is fixed to the needle base. All seven NiTi wires are straight at room temperature and have a smooth surface ($R_a = 0.17 \mu\text{m}$, average of two measurements with a Mitutoyo SurfTest SJ-301). The wires were cut to length using pliers and did not undergo any further machining afterwards.

Three different kinds of rings are used to hold the needle wires together: an interlocking ring, an alignment ring and steel rings (Figure 4). The interlocking ring (aluminium; $d = 1.2$, $l = 2.0$ mm) is located at the needle tip and is used to align the wires relative to each other. This ring has seven individual holes ($d = 0.3$ mm) through which the wires are fed. The radial distance between the center axis of the interlocking ring and each of the centers of the six outer holes is 0.375 mm. The central wire is glued to the center hole of the interlocking ring at the needle tip using a two-part epoxy adhesive, whereas the six outer wires can slide through the concentrically arranged holes in the ring. The material at the outer periphery of the interlocking ring was trimmed around the six holes to reduce its resistance to the forward motion of the needle.

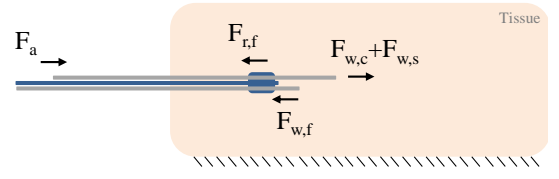
The seven-holed alignment ring (aluminium; $d = 3$ mm, $l = 2$ mm, $d_{\text{holes}} = 0.3$ mm) has an asymmetric cross section and is placed behind the interlocking ring. The alignment ring is fixed to a reference point (e.g., the needle base or the tissue, etc.) to make sure that the radial orientation of the needle relative to the reference point is as desired when the needle is first inserted in the tissue. All seven wires can slide freely through their allocated holes in the alignment ring.

Between the alignment ring and the needle base the needle wires are held together by five stainless steel rings ($d_{\text{in}} = 0.9$ mm, $d_{\text{out}} = 1.0$ mm, $l = 2$ mm) that are placed with a uniform spacing along the needle body. The seven NiTi wires are fed through the steel rings and can slide freely. During assembly special care was taken to prevent the individual wires from twisting when fed through the steel rings.

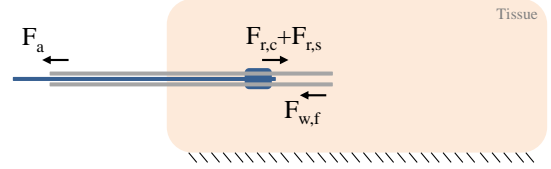
D. Forward Motion and Steering of the Needle

1) *Forward Motion*: The needle can be advanced by first pushing the needle wires forward one after the other or in pairs, followed by pulling on all wires simultaneously (Figure 5). This sequence will henceforth be referred to as ‘cycle’.

In the first step of a cycle, the six movable wires are advanced (Figure 5a) whereby the cutting and sliding force of the advancing wire(s) are compensated by the friction force



(a) Needle wires are pushed forward by actuator (F_a). The static friction on stationary needle wires ($F_{w,f}$) compensates for the necessary cutting and sliding force ($F_{w,c} + F_{w,s}$) of advancing wire(s).



(b) Advancing interlocking ring and central wire by simultaneously pulling ($6 \cdot F_a$) on all six movable needle wires. The force required for moving the ring and central wire forward ($F_{r,c} + F_{r,s}$) is compensated by the static friction force of the six wires ($6 \cdot F_{w,f}$).

Fig. 5: The needle is moved through the tissue by repeating the two steps shown in (a) and (b). The figure shows the scenario in which the tissue sample is stationary and the needle base is movable.

of the stationary wires. In the ideal case that the forces of the advancing wire(s) are fully compensated for, no net movement of the needle occurs. This ideal case can be expressed in a simplified way by:

$$m \cdot (F_{w,c} + F_{w,s}) \leq m \cdot F_a \leq n \cdot F_{w,f} + F_{r,f}, \quad (1)$$

where m represents the number of simultaneously advancing wires and n the number of stationary wires. $F_{w,c}$ is the cutting and $F_{w,s}$ the sliding component of the force that one wire has to overcome to advance through the tissue. $F_{w,f}$ and $F_{r,f}$ are the static friction force of one stationary wire and the interlocking ring, respectively. F_a represents the actuator force exerted on one wire.

In the second step of the cycle, pulling on all six wires simultaneously advances the interlocking ring and the central wire deeper into the tissue as shown in Figure 5b. In the ideal case, the force required for advancing the interlocking ring is fully compensated by the static friction force between the wires and the tissue which can be expressed in the following simplified way:

$$F_{r,c} + F_{r,s} \leq 6 \cdot F_a \leq 6 \cdot F_{w,f}, \quad (2)$$

where $F_{r,c}$ and $F_{r,s}$ are the cutting and sliding components, respectively, of the force needed to move the ring through the tissue.

By repeating the sequence of these two steps, the needle is moved through the tissue. Slip of the needle against the tissue occurs when either of (or both) inequality equations 1 and 2 are not satisfied.

2) *Steering*: Steering is achieved by creating an asymmetric tip shape that will make the needle deflect in the desired direction. In our prototype this is done by creating an offset between two adjacent needle wires. In doing so, the tip of the two needle wires forms a ‘quasi’ bevel-tip (Figure 6). The angle of this bevel can be controlled by changing the offset between the two adjacent wires (called ‘bevel offset’ (BO), Figure 6). When the adjacent needle wires are simultaneously advanced to the desired depth (called henceforth the ‘dynamic offset’ (DO)), they deflect in the direction of the quasi bevel. For steering the needle in a desired direction a quasi bevel-tip configuration is formed on two wire pairs in such a way that the directions in which the two pairs deflect complement one another in achieving steering (Figure 7). The following steps outline the actuation scheme:

- i) A quasi bevel-tip corresponding to the desired steering direction is formed on two complementary needle wire pairs.
- ii) The first quasi bevel wire pair is advanced. The asymmetric tissue interaction forces arising due to the quasi bevel-tip on the wire pair cause it to deflect and cut a path in the substrate.
- iii) The second quasi bevel wire pair is advanced. This reinforces the trajectory cut in the substrate by the first needle wire pair.
- iv) The remaining two needle wires are pushed forward following the trajectory cut by the complementary wire pairs in steps ii) and iii).
- v) A pull force is exerted on all needle wires simultaneously to move the central wire and the interlocking ring which are fixed to the needle base further inside the gelatin along the cut trajectory.

By repeating steps ii) - v) the needle can be moved along a curved trajectory. The steering direction is determined by the wire pairs on which the quasi bevel-tip is created (i.e. step i)). In our six-segment design, steering to the left can be achieved with a quasi bevel-tip on the wire pairs 1-6 and 4-5 (as shown in Figure 7). Steering to the right is facilitated by a quasi bevel-tip on the complementary wire pairs 1-2 and 3-4. For up and down steering the segment pairs 2-3 and 5-6 are used with segments 2 and 6 protruded for upward and 3 and 5 for downward steering.

III. DESIGN OF THE ACTUATION UNIT

A. Design Considerations

1) *Functional Objectives*: In order to investigate the working principle of our steerable needle an actuation unit capable of moving the needle wires forward and backward was designed. A key objective in the development of this actuation unit was to design it in such a way that different actuation settings as well as variations in the design of the needle

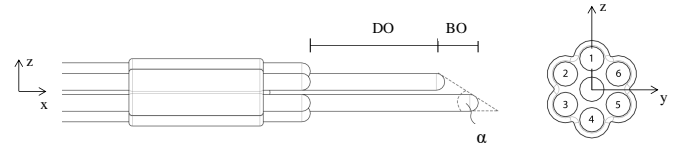


Fig. 6: Schematic representation of the needle tip. The side view (left) shows how a quasi bevel-tip with angle α is formed by creating a ‘bevel offset’ (BO) between the adjacent needle segments 5 and 6 (see front view figure on the right side). The ‘dynamic offset’ (DO) represents the distance a segment pair is pushed forward.

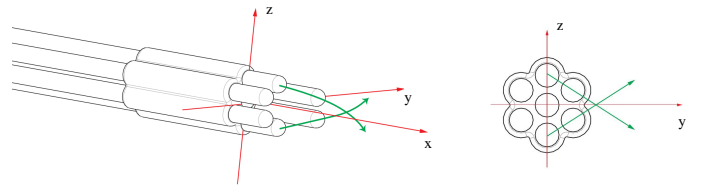
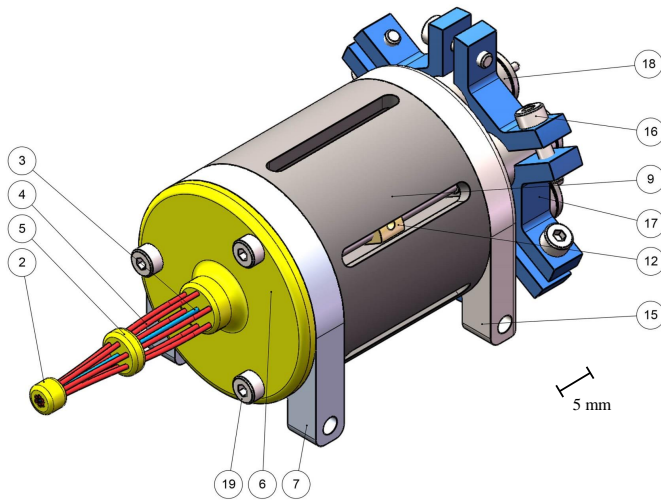


Fig. 7: Figure showing the needle tip shape for steering to the left. Green arrows indicate direction in which the two segment pairs deflect when pushed forward.

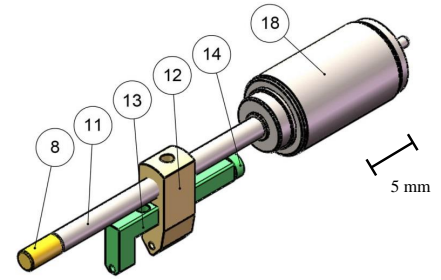
can be investigated. The main functional requirements for the actuation unit are listed below.

- i) The actuation unit has to be capable of moving individual wires as well as multiple wires at the same time. Furthermore, the sequence in which the wires are actuated should be variable.
- ii) The needle wires have to be moved forward and backward which requires a power train that can provide linear motion.
- iii) The actuation unit should allow for the wires to be moved forward and backward over a distance of at least 20 mm to allow comparing our results to previous work [31], [46].
- iv) The velocity with which the wires are moved should be adjustable so that it is possible to compare our results with those in previous studies [31]. For this reason, it should be possible to move the wires with a speed of up to 15 mm/s and to change the speed in increments of at least 1 mm/s.
- v) A positioning resolution for the wires of at least 0.1 mm is desired to be able to adjust the angle of the quasi bevel-tip accurately.
- vi) It should be possible to investigate different wire materials and diameters with the same actuation unit.
- vii) The actuation unit should be reconfigurable to allow investigating different needle designs, for example a needle with three, four or five instead of six wires.

2) *Size and Weight Considerations*: In designing and selecting the components for the actuation unit our goal was



(a) Schematic overview of the actuation unit.



(b) Schematic close-up view of the power train.

Fig. 8: Schematic overview of the actuation unit (a) and the power train (b) for actuating one of the six needle wires. (2), (5): Secondary tube holders; (6): Primary tube holder; (3), (4): Tubes for the NiTi wires; (7): Bearing housing; (8): Leadscrew bearing; (9): Slider housing; (11): Leadscrew; (12): Slider; (13); (14): Buckling support; (15): Motor housing; (16): Screw for clamping the motors; (17): Motor clamp; (18): Stepper motor.

for the final design to be as small and lightweight as possible and thereby explore the feasibility of integration into a hand-held device. Moreover, since the forward motion principle of our needle (see Figure 5) holds when either the tissue or the actuation unit (i.e., the needle base) is fixed, one possible way of evaluating the performance of our needle would be to design the actuation unit to be movable while the tissue is stationary. In the same way, the tissue could be devised to be movable and the actuation unit stationary. In both scenarios, it is desired to keep the influence of the inertia of the movable part as well as the friction between the ground and the movable part on the forward motion of the needle as small as possible. If small tissue samples are used, a fixed actuation unit might be advantageous, however, if 3D steering in a large and heavy tissue sample is to be investigated, a movable actuation unit might be the preferred option. Thus, designing the actuation unit to be lightweight allows it to be used in both scenarios.

B. Conceptual Design Process

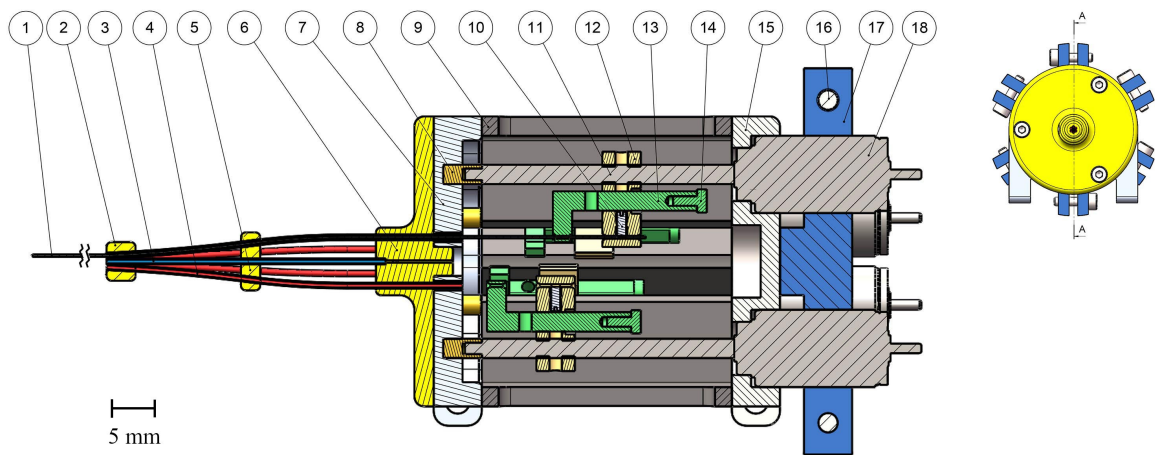
The three main challenges in designing the actuation unit were the design of the power train responsible for moving the needle wires, the design of the housing of the power train and the design of a mechanism to prevent buckling of the needle wires. First, the power train along with a suitable controller were designed and components to be purchased were selected, followed by iterative design of the housing and the buckling prevention mechanism.

1) Power Train and Controls: For the design of the power train the actuators were selected first. In order to keep the

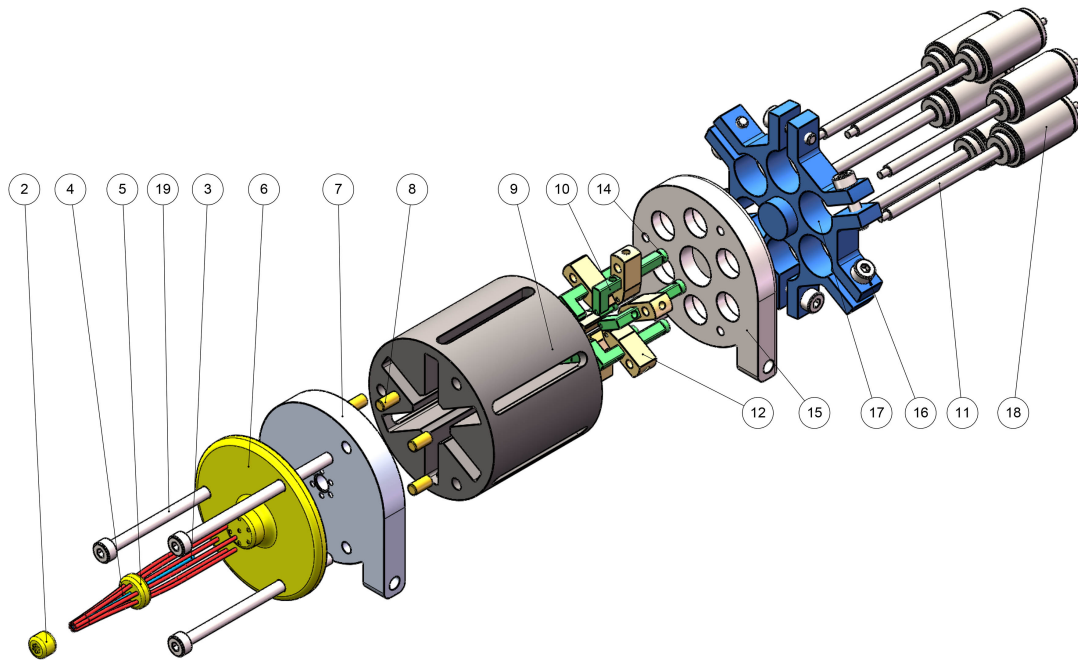
experimental setup simple, we opted for electric actuators whereas hydraulic and pneumatic actuators were not considered. Achieving linear motion directly by means of linear actuators seemed promising at first, yet was discarded later due to limited availability of such actuators in small dimensions (i.e., less than 10 mm in diameter). Rotational electric motors, on the other hand, were found to be widely available in small dimensions and could easily be combined with a transmission to achieve linear motion. Out of the many transmissions and mechanisms capable of translating rotational to linear motion, a leadscrew-slider mechanism was favored because the motor axis could be placed in-line with the transmission axis, rather than perpendicular to it as, for example, in a crankshaft mechanism or a pinion-and-rack transmission, or off-axis, as in wobble plate mechanisms. Placing motor and transmission on the same axis allowed for a compact overall construction of the power train.

For the control of the motors a simple solution was sought after. Since stepper motors can provide high positioning accuracy while being operated in an easy to control feed-forward fashion this type of motor was selected. The Arduino platform was chosen as controller because of its user friendliness and because the authors had prior experience with software design for the Arduino micro-controller.

2) Housing: The design of the parts comprising the actuation unit housing was an iterative process focused on making the housing as compact and lightweight as possible. For this reason, lightweight materials were used unless the function of the part required a different material.



(a) Cross section view of the actuation unit. Only one of the six movable needle wires is shown.



(b) Exploded view of the actuation unit. The needle wires are not shown.

Fig. 9: Cross section (a) and exploded (b) view of the actuation unit showing the individual parts. (1): NiTi wire (only one shown); (2), (5): Secondary tube holders; (6): Primary tube holder; (3), (4): Tubes for the NiTi wires; (7): Bearing housing; (8): Leadscrew bearing; (9): Slider housing; (10): Set screw to clamp NiTi wire; (11): Leadscrew; (12): Slider; (13); (14): Buckling support; (15): Motor housing; (16): Screw for clamping the motors; (17): Motor clamp; (18): Stepper motor; (19): Bolt for assembling the parts.

Special attention was paid to the design of the slideway for the leadscrew-slider mechanism (i.e., the ‘slider housing’, see Figure 9b). In several design iterations the possibility of allowing for visual position control of the slider was explored.

Furthermore, ways of ensuring smooth sliding motion of the slider in the slideway (i.e., by testing different material combinations and slider geometries) were investigated.

3) *Buckling Prevention Mechanism:* The required range of motion of the sliders of 20 mm as stated in section III-A1 meant that the unsupported length of the needle wires inside the actuation unit could reach up to 20 mm. By manually inserting the needle wire into gelatin it was established that the unsupported length of the wire should not be more than 10 mm in order to avoid buckling of the wire. Generally, buckling of the needle wires could be prevented by a cylindrical structure that is placed around the needle wire. Since the range of motion of the sliders was to remain 20 mm, the buckling prevention mechanism would also have to adjust its length during forward or backward motion of the sliders. This could, for example, be accomplished by a telescoping tube or a coil spring placed around the needle wires. However, both of these were discarded because they were either too complex to manufacture (i.e., in the case of the telescoping tube) or would create an inconstant force on the slider with a magnitude dependent on the slider position (i.e., in the case of a coil spring). Another approach to preventing wire buckling was to reduce the unsupported length of the wires rather than covering the entire wire length. The mechanism designed following this reasoning consisted of an additional part holding the needle wire. This added part was attached to the brass slider, yet able to move relative to the slider as it approached the inner walls of the actuation unit, making sure the range of motion of the slider was not reduced.

C. Description of the Final Design

1) *Power Train and Controls:* The power train for moving the needle wire forward and backward consisted of a stepper motor connected to a leadscrew-slider mechanism which translates the rotational motion of the motor to linear motion (Figure 8b). Bipolar stepper motors (Faulhaber AM0820) with a step angle of 18° in full step mode in conjunction with a 28 mm long M2 leadscrew (pitch = 0.2 mm) were selected. This motor-leadscrew assembly was chosen because it is both small ($d = 8$ mm), powerful (up to 1.5 N push force), capable of providing the desired positioning resolution (i.e., 0.01 mm in full step mode) and can operate over a large range of velocities (up to 25 mm/s at nominal voltage). The leadscrew drove a polished brass slider which was able to slide along an aluminium slideway to keep losses due to friction as small as possible. Each needle wire was fixed to the corresponding slider with a set screw (see Figure 9a). The maximum travel distance of the slider along the leadscrew, and thereby that of the needle wires, was 20 mm. The bearing arrangement of the leadscrew comprised a roller bearing in the stepper motor as well as a brass sliding bearing on the free end of the leadscrew.

To be able to control the position and travel speed of each wire individually, each of the six movable wires was actuated by a power train as described in the previous paragraph. The six stepper motors were controlled using an Arduino MEGA 2560 micro-controller and six motor driver carriers (Texas Instruments DRV8834) in a feed-forward manner. The software and user interface were created using the Arduino IDE (v.1.6.5). A schematic overview of the code structure is shown in appendix B.

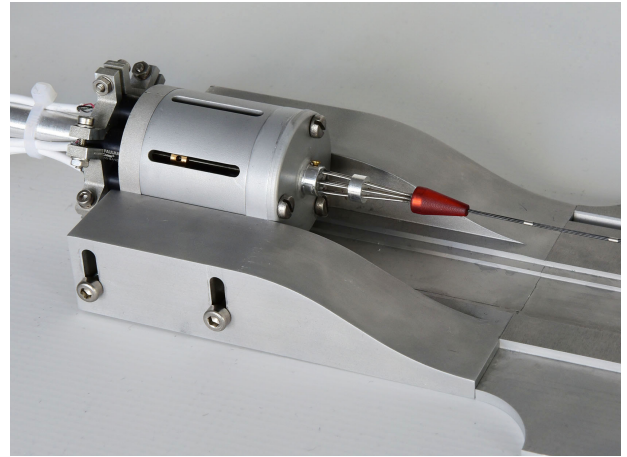


Fig. 10: Close-up photograph of the actuation unit fixed to the test rig.

2) *Housing:* The main body of the actuation unit housing consisted of four cylindrical parts (i.e., the motor housing, the slider housing, the bearing housing and the primary tube holder) held together by three M3 bolts (Figure 8a, 9b). The six stepper motors were concentrically positioned around the central axis of the actuation unit and screwed to the motor housing. The motors were placed as close to the central axis as possible to keep the overall size of the actuation unit small. Loosening of the motors was prevented by the six clamps of the motor clamp part (Figure 8a) which was glued to the motor housing. The slider housing consisted of six rectangular slots which acted as the slideway for the six brass sliders. Furthermore, the slider housing comprised six longitudinal slots on the outside of the part to allow for visual position control of the sliders. The bearing housing held the six sliding bearings for the bearing arrangement of the leadscrew (Figure 9a). Furthermore, it contained two holes at the bottom of the part that, together with the same kind of holes in the motor housing, could be used for either fixing the actuation unit to the ground or attaching wheels to it. The primary tube holder contained six concentric longitudinal holes holding six tubes through which the movable needle wires were guided to the front of the actuation unit. It further contained a longitudinal hole in its center through which the central needle wire (see section II-C) was fed. The central needle wire was clamped to the primary tube holder with a set screw.

Stainless steel tubes were attached to the main body of the actuation unit for smooth guiding of the movable needle wires to the central axis of the actuation unit (Figure 9a). To allow guiding the steel tubes toward the center, two secondary tube holders containing holes drilled at an angle were used. Because of the wall thickness of the steel tubes, the needle wires could not be guided close enough to the central axis to be touching each other. Since this could potentially lead to jamming of the steel rings holding the needle wires together (see section II-C) as the rings approach the front secondary tube holder, a 3D printed cone was glued to this tube holder (see Figure 10).

All the manufactured parts of the actuation unit except for the sliding bearings, the sliders and the tubes were made from aluminium in order to keep the mass of the actuation unit as low as possible. The total length of the actuation unit was approximately 85 mm and its diameter 40 mm.

3) *Buckling Prevention Mechanism*: In order to reduce the unsupported length of the needle wires inside the actuation unit, an L-shaped buckling support part was designed featuring a hole at its short end through which the needle wire can slide. The buckling support was slidably connected to the brass slider by means of a rectangular hole whose shape prevented rotation of the buckling support relative to the slider (Figure 8b). Because the L-shaped buckling support protruded from the slider and could move forward and backward relative to it, the buckling support always touched the inner wall of the bearing and motor housing first. Therefore, pushing the buckling support to either of these walls forced it to slide through the hole in the slider, thereby decreasing the unsupported length of the needle wire (Figure 11). Using this mechanism it was ensured that the unsupported length of the needle wire was never more than 10 mm which corresponds to half of the total range of motion of the slider. In order to ease the process of exchanging the needle wires, a hole in the buckling support part allowed for the set screw used for clamping the needle wire to be unfastened and the wire replaced without having to disassemble the slider and buckling support parts (see Figure 9a).

IV. EXPERIMENTAL VALIDATION

A. Dependent and Independent Variables

We performed two separate experiments in order to assess the performance of the prototype in forward motion and in steering. In the forward motion experiment (Experiment 1) the dependent variable was the slip between the needle and the substrate. We defined slip as the ratio of the measured to the theoretical travel distance of the needle. In the steering experiment (Experiment 2) the steering curvature of the needle served as the dependent variable.

In Experiment 1, the independent variable was the number of needle segments that are advanced simultaneously. In Experiment 2, the independent variables were the ‘bevel offset’ (BO), the ‘dynamic offset’ (DO, Figure 6), and the steering direction. BO was defined as the offset created between two neighboring needle segments that are advanced simultaneously. DO was defined as the distance to which the simultaneously advancing needle segments are moved forward (or backward) and thus represents the maximum theoretically possible travel distance of the needle in each cycle.

B. Hypotheses

According to the model presented in II-D1 we expected slip to be inversely proportional to the ratio between the number of stationary and moving needle wires. In other words, we expected slip to increase with the number of simultaneously actuated needle wires.

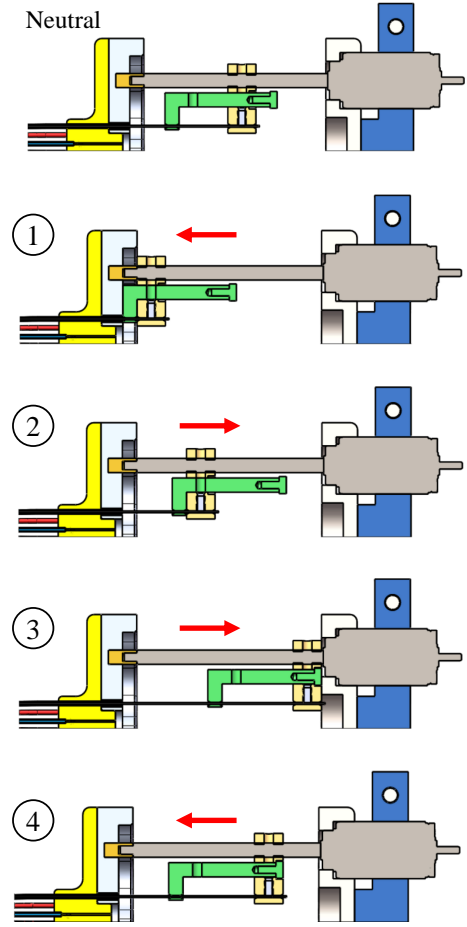
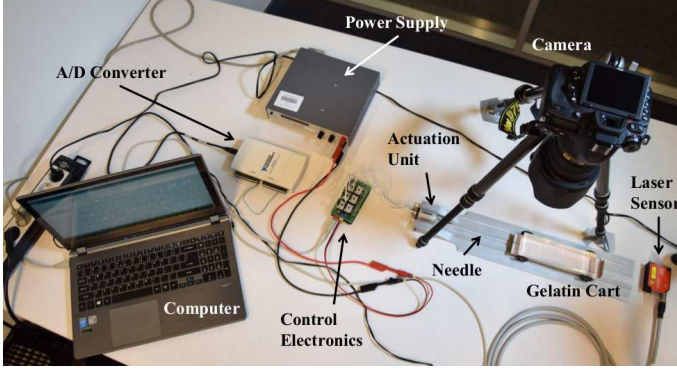


Fig. 11: Schematic representation of the buckling prevention mechanism. The arrows indicate the direction of motion of the slider. When the L-shaped buckling support touches either of the walls, it slides through the hole in the slider thereby making sure that the unsupported length of the needle wire is never more than 10 mm (i.e., half the total range of motion of the slider).

For the steering curvature experiment, we hypothesized that curvature is proportional to BO, consistent with experimental and analytic works on bevel-tip needles showing that smaller bevel angles lead to larger steering curvatures [39], [40]. With respect to DO, we expected a proportional relationship between DO and steering curvature, as DO can be compared to the length of a cantilevered beam subject to a load at its tip.

C. Experimental Setup

The experimental setup for both Experiments 1 and 2 consisted of the actuation unit, a test rig and data acquisition instruments (Figure 12).



(a) Overview of the experimental setup.



(b) Close-up photograph of the test rig.

Fig. 12: Experimental setup used for Experiments 1 & 2.

1) *Test Rig*: The actuation unit was mounted on an aluminium base plate using four bolts. A lightweight aluminium cart (210 x 50 mm, 28 g) was designed to carry a gelatin phantom. Actuating the needle in the reciprocating manner described in section II-D1 moved the gelatin cart toward the fixed actuation unit. A millimeter paper grid was fitted to the inside of the cart to serve as a distance reference during the experiments. The movement of the wheels of the cart was laterally constrained by a groove in the base plate.

2) *Data Acquisition*: During the experiments the position of the cart was measured using a laser proximity sensor (Micro-Epsilon optoNCDT1302-200, range: 200 mm, resolution: 0.1 mm). The sensor was positioned behind the base plate, parallel to the back side of the cart. The laser data was collected using an NI USB-6211 16-bit data acquisition unit in conjunction with LabVIEW 2013 at a sampling frequency of 5 Hz.

For Experiment 2, videos of the experimental trials were recorded using a Panasonic HC-V250 video camera. At the end of every experimental trial of Experiment 2 a top-down view photograph of the needle inside the gelatin phantom was taken with a Nikon D750 camera mounted on a tripod.

D. Experimental Design

The concentration of the gelatin phantom was 4 wt% for all experiments. The needle segments were actuated at a speed of 2 mm/s. The total number of cycles executed by the Arduino software was chosen to result in a theoretical needle insertion depth of 120 mm in all experimental trials of both Experiment 1 and 2. The combined weight of the cart and gelatin phantom was kept constant throughout the experiments (mean = 214.66 g, standard deviation = 1.69 g). The needle insertion depth of the needle at the start of the experiments was approximately 25 mm.

1) *Experiment 1*: The number of simultaneously actuated needle segments was varied between one ('single') and two ('paired'). The DO was 4.0 mm for both single and

TABLE I: Experimental Conditions for Experiment 2 (BO: Bevel Offset, DO: Dynamic Offset).

Condition No.	BO [mm]	DO [mm]	Direction
1	3.6	2.0	left
2	3.6	2.0	right
3	1.8	4.0	left
4	1.8	4.0	right
5	0.9	4.0	left
6	0.9	4.0	right
7	3.6	4.0	left
8	3.6	4.0	right
9	3.6	6.0	left
10	3.6	6.0	right

paired actuation tests. Needle segments were actuated counter clockwise when viewed from the needle tip starting with segment '1' in single and segment pair '1-2' in paired actuation (see Figure 6). Six trials were conducted for both the single and the paired conditions in a randomized order over the course of one day.

2) *Experiment 2*: The BO was varied between 0.9, 1.8 and 3.6 mm (derived from bevel angles of 20, 10 and 5 degrees respectively (see Figure 6)). For the DO the offsets 2.0, 4.0 and 6.0 mm were tested. The steering direction was varied between left and right. Of the 18 possible combinations of these conditions (3 BO x 3 DO x 2 directions), a set of ten conditions was chosen in such a way that BO and DO were varied from a common baseline (BO = 3.6 mm, DO = 4.0 mm) for both directions (Table I). Each condition was repeated five times in a randomized order over the course of eight days. When steering to the left, the segment pairs were actuated clockwise, with pair '6-5' actuated first. For steering to the right, the segment pairs were actuated counter clockwise, with pair '1-2' actuated first.

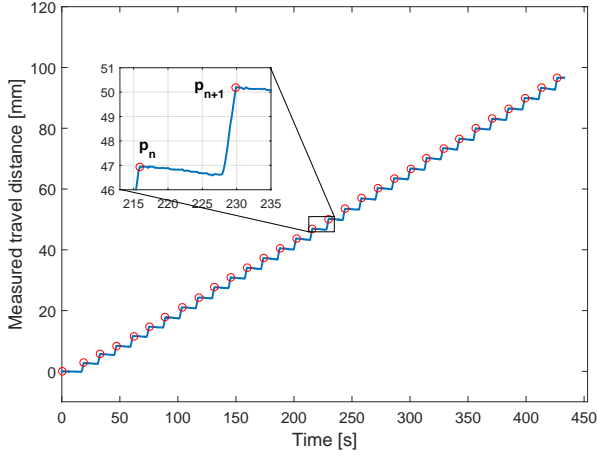


Fig. 13: Example of travel distance of the needle over time for single actuation mode. Peaks (p) denote the starting point of an actuation cycle.

E. Gelatin Preparation

The gelatin phantom was prepared by mixing Dr. Oetker gelatin powder with boiled water of about 70 - 80 °C. The mixture was stirred until all of the gelatin powder had been dissolved. The liquid gelatin was then poured into smaller containers and stored overnight at 5 °C. For each day of measurements a new batch of gelatin was made. Before each experimental trial a gelatin block of 50 x 170 x 30 mm (width x length x height) was cut out of the containers.

F. Experimental Procedure

The gelatin block was placed in the cart and the needle manually inserted about 25 mm deep inside the phantom. After selecting the desired settings in the Arduino software, the laser sensor and video camera were switched on and the experimental trial started. In the steering experiment a photograph of the final position of the needle inside the gel was taken at the end of each trial. The needle was then removed from the gelatin and cleaned with warm water.

G. Data Analysis

1) *Experiment 1:* The raw data curves of the cart movement collected by the laser sensor were imported in MATLAB (version 2014b) and shifted so that they all had 0 mm as a common starting point of the motion. This was done by subtracting the distance measured at the first data point from all data points of the experimental trial. Next, the maxima (p) of each actuation cycle were extracted. The slip ratio s_n was calculated as

$$s_n = 1 - \frac{d_{m,n}}{d_{th}}, \quad (3)$$

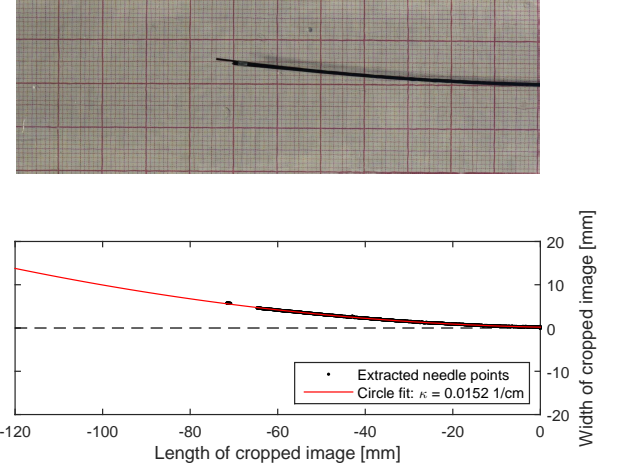


Fig. 14: Example of the data analysis procedure for determining the steering curvature in Experiment 2. The figure shows the cropped photograph (top) and the extracted curved needle with the fitted circle (bottom) for experimental trial no. 4 of condition 8 (i.e., BO = 3.6 mm, DO = 4.0 mm, direction: right).

where d_{th} is the specified DO, or in other words, the theoretical travel distance for each cycle, and $d_{m,n}$ is the measured travel distance for each cycle given by

$$d_{m,n} = p_{n+1} - p_n, \quad (4)$$

where n represents the actuation cycle (see Figure 13). The slip ratio was derived under the assumption that no deviation from the straight path of the needle occurred.

The mean insertion speed (\bar{v}_{in}) of the needle for single and paired actuation was calculated as

$$\bar{v}_{in} = \frac{p_{end} - p_2}{t(p_{end}) - t(p_2)}, \quad (5)$$

where p_{end} represents the last peak of the trial and $t(p_{end})$ the corresponding time.

One data set of the single actuation trials was removed because the laser sensor data was erroneous.

2) *Experiment 2:* The photographs of the final position of the needle inside the gelatin were cropped to a size of 40 x 120 mm based on the millimeter paper grid in such a way that the 25 mm of manual needle insertion were removed. For each of these cropped images a scaling factor was calculated by dividing 120 mm by the length of the image in pixels. Utilizing the MATLAB image processing toolbox, the cropped images were then converted to binary images after which a number of morphological operations were used to extract the center line of the needle from the images and remove noise.

A circle was fitted to the extracted needle center line based on the circle equation in one plane:

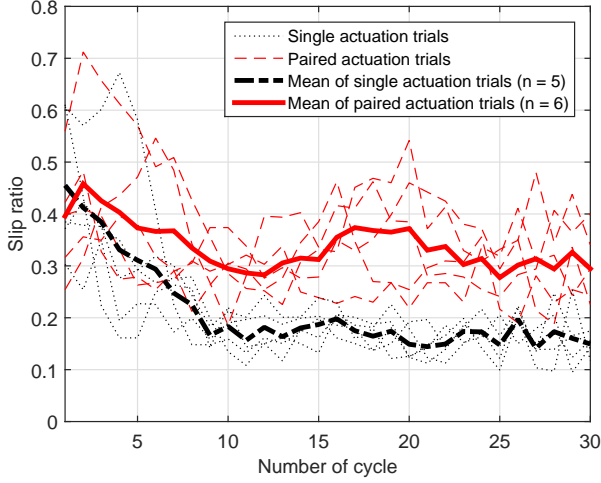


Fig. 15: Results of Experiment 1 showing the slip ratio of the needle in single and paired actuation.

$$\mathbf{x}^T \mathbf{x} + \mathbf{b}^T \mathbf{x} + c = 0, \quad (6)$$

where $\mathbf{x}, \mathbf{b} \in \mathbb{R}^2$. Using the extracted needle data points (\mathbf{x}), the fitted circle radius r_{fit} was obtained for each experimental trial and the curvature κ calculated by

$$\kappa = (r_{fit})^{-1}. \quad (7)$$

The scaling factor was used to convert κ to 1/cm (Figure 14). Note that κ was obtained under the assumption that the needle only moved in one plane (i.e. the steering plane).

Both cropped images and fitted circles were manually checked to make sure that steering occurred in the imposed steering direction. For all trials in which this was not the case steering was considered ‘unsuccessful’ and κ was set to 0.

V. RESULTS

A. Experiment 1

Single actuation led to less slip during needle insertion compared to paired actuation (Figure 15). Furthermore, the slip ratio in single actuation showed less variability than the slip ratio in paired actuation. Specifically, the mean slip ratio across all actuation cycles was 0.21 for single actuation ($n = 5$) and 0.34 for paired actuation ($n = 6$). In the single actuation trials the slip ratio was highest in the first few cycles, and stabilized after about nine cycles. The slip ratio in paired actuation showed a similar trend.

The mean total travel distance of the needle in the single actuation trials was 94.6 mm ($n = 5$), and 79.4 mm in paired actuation ($n = 6$).

The mean insertion speed of the needle was 0.23 mm/s ($n = 5$) in single actuation, and it was 0.33 mm/s ($n = 6$) in paired actuation.

B. Experiment 2

Steering curvatures were larger for steering to the right than for steering to the left (Figure 16). Steering to the left was unsuccessful in 10 out of 25 trials, with conditions 7 and 9 showing the poorest steering performance (4 out of 5 unsuccessful). In conditions 3 and 5, one unsuccessful trial occurred. Steering to the right was successful in all trials.

Variability between trials of the same condition increased with increasing offset (for both BO and DO) when steering to the right.

The largest mean curvature was achieved for condition 2 ($\kappa = 0.0184$ 1/cm, Table II).

VI. DISCUSSION

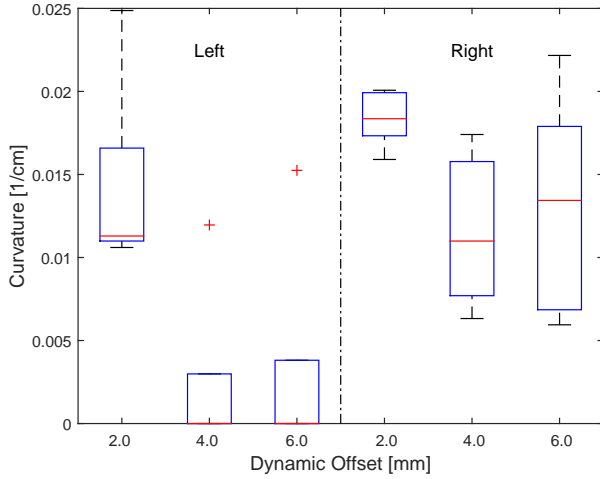
A. Steerable Needle Concept

In this study we have presented a novel approach for the design of a steerable needle inspired by the ovipositor of parasitic wasps. Steering in various directions by means of a reconfigurable tip and preventing needle buckling through near zero net-force insertion are two features of the wasp ovipositor that have already been incorporated in steerable needle designs showing promising results [30], [31]. While previous work has mainly been directed toward probes for neurosurgery (smallest probe diameter reported: $d = 4$ mm, [32]), the goal of this study was to develop a needle that both utilizes the ovipositor mechanism and that has a maximum diameter of 2 mm, so that it can be used in percutaneous interventions. Our needle prototype had a diameter of 1.2 mm. This small size of the needle was achieved by using wires as needle segments instead of cylindrical sectors and external rings instead of internal interlocking of the segments. Moreover, instead of introducing a bevel-tip, the steering mechanism in our prototype was based on the creation of a ‘quasi’ bevel between adjacent segments, allowing the bevel shape (and therefore the steering angle) to be varied during the procedure. Such a dynamically variable bevel shape might allow for more accurate control of the steering direction compared to a needle with a fixed bevel.

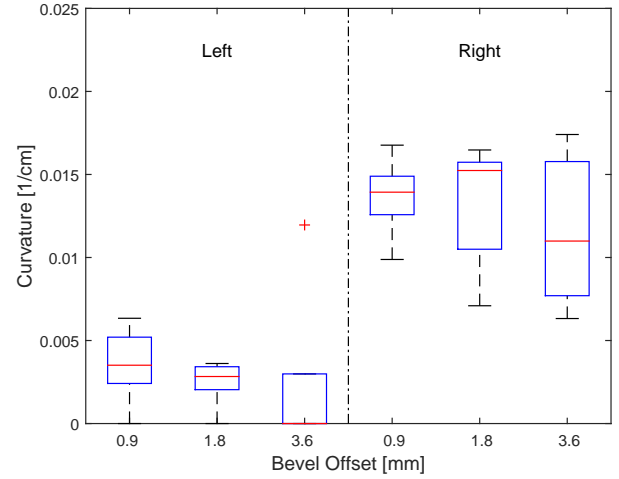
B. Interpretation of Results

1) *Experiment 1*: The slip ratio in the single actuation trials was higher than in paired actuation, in line with our hypothesis. This can be explained by the higher ratio between stationary and moving wires in single actuation (i.e., 5) as compared to paired actuation (i.e., 2).

The stabilization of the slip ratio observed after a number of cycles indicates that a certain insertion depth is needed for the needle to move forward with constant slip. The mean travel distance that is required to reach this constant slip region was calculated to be approximately 24.7 mm (i.e., sum of the mean travel distances of the first 9 cycles) for single actuation. In a verification experiment consisting of five trials, the slip during single-actuated forward motion of the needle with an initial needle insertion depth of 50 mm was investigated. It was confirmed that deeper manual insertion of the needle at the start of the trial results in constant slip throughout the experiment (Figure 17). This is in line with previous findings showing that



(a) Results of the conditions with constant bevel offset (BO = 3.6 mm). Five trials were performed for each condition.



(b) Results of the conditions with constant dynamic offset (DO = 4.0 mm). Five trials were performed for each condition.

Fig. 16: Results of Experiment 2 in which steering performance was tested for ten different conditions (see Table I).

the friction force on a needle increases with insertion depth while the cutting force stays approximately constant [44].

The greater variability observed in the paired actuation measurements is thought to be due to random deflection of the wire tips of the actuated wire pair as they are advanced out of the interlocking ring. This random deflection could lead to the wires touching in some trials and bifurcating in other trials. If the wires bifurcate, they generate more frictional resistance than if they stay in contact with each other. Therefore, the resistance generated by the wires, and thereby the required force for advancing the wire pair, can differ between trials which explains the inter-trial variability. In single actuation there is no such interaction between the needle wires.

A slip ratio of approximately 0.7 was reported previously when using a four-part needle with a diameter of 2 mm inserted into a Dr. Oetker gelatin (8wt%) in a single actuation manner (DO = 4.0 mm, insertion speed: 4 mm/s, [31]). The considerably lower slip found in the present study (i.e., 0.21 for single and 0.33 for double actuation) can be attributed to the lower gelatin stiffness used (i.e. 4wt%) and/or the smaller diameter of the segments cutting through the gelatin (i.e., 0.25 mm in our prototype as compared to 0.5 mm). This is consistent with previous work showing that peak axial needle insertion force increases with needle diameter [47].

If only the slip ratio is considered, single actuation outperforms paired actuation. However, the necessity of reducing slip in a needle procedure has not been established yet. Slip makes the actual insertion depth unpredictable, yet this could be overcome by visually monitoring the position of the needle tip. If such a visual feedback system is in place, it is likely that paired actuation with its significantly faster insertion speed (45% faster than single actuation) is to be

TABLE II: Mean curvature for each condition of Experiment 2.

Condition No. (BO [mm], DO [mm], Direction)	Mean κ [1/cm]
1 (3.6, 2.0, L)	0.0143
2 (3.6, 2.0, R)	0.0184
3 (1.8, 4.0, L)	0.0025
4 (1.8, 4.0, R)	0.0132
5 (0.9, 4.0, L)	0.0036
6 (0.9, 4.0, R)	0.0137
7 (3.6, 4.0, L)	0.0024
8 (3.6, 4.0, R)	0.0116
9 (3.6, 6.0, L)	0.0030
10 (3.6, 6.0, R)	0.0130

favorable to reduce the overall procedure time. The effect of slip on tissue damage has - to our knowledge - not been studied yet and should be factored in when evaluating the two actuation methods.

2) *Experiment 2*: Contrary to our hypotheses, deflection of the needle was found to be inversely proportional to the dynamic offset (DO) and the bevel offset (BO); that is, deflection was proportional to the quasi bevel angle α . A possible explanation is that with larger offsets the wires tend to bifurcate more, causing the individual wires of the segment pair to deflect irregularly. When this happens, the segment pair can lose its quasi bevel configuration (see Figure 6) and it is therefore likely that the segment pair does not deflect in the desired direction anymore. A proportional relationship between curvature and bevel angle was also reported in Frasson

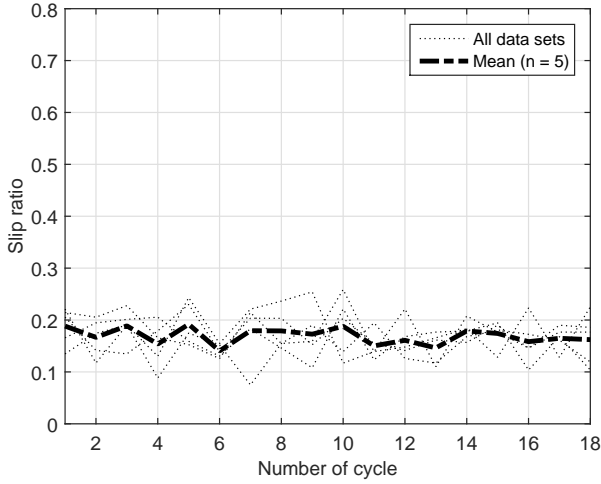


Fig. 17: Results of the validation experiment for single actuation in which the initial insertion depth was 50 mm.

et al. [38], in which the authors suggested that this unexpected relationship might be due to their probes having a considerably larger diameter (i.e., 9 & 12 mm) than regular needles. Irregular deflection of the wires of the actuated segment pair can also explain the larger variability seen in the conditions with larger BO and DO. Consequently, the smallest BO combined with the smallest DO of our experimental array is expected to yield the best results with our current prototype since this is the condition for which bifurcation is minimal.

The considerably higher curvatures achieved when steering to the right compared to steering to the left might have been caused by a bias in the needle wires. The needle bends to the right when relaxed (likely to be caused by the wires not being perfectly straight), yet it is unclear to what extent this pre-curvature of the needle affects steering. Furthermore, the gelatin cart might cause this bias, as the wheels were found to come loose over time. This could also explain the outliers found in the first trial of conditions 7 and 9 which were both performed on the first day of the steering experiment.

Due to bifurcation of the needle segments in the current prototype, it was not possible to establish a systematic relation between the BO & DO and the steering curvature. Together with the directional bias in our experimental setup as well as the low number of experiments this means that the present study can only serve as an initial proof of principle of the steering capability of this new needle concept.

In order to show that our needle can be steered in various directions without axially rotating the needle, we conducted three experimental trials in each of which the steering direction was changed from left to right during needle insertion with BO = 0.9 mm and DO = 2.0 mm. It was found that the steering direction of the needle could be changed from left to right in all three trials (Figure 18).



Fig. 18: Photograph of the final position of the needle inside the gelatin in an experimental trial in which the steering direction was changed from left to right.

C. Limitations

1) *Experiment 1:* In the data analysis we assumed that needle deflection would occur only in the steering plane (i.e. horizontally). However, visual observation revealed that the needle also tended to deflect upwards. This upward deflection was not measured, yet appeared to occur in all experimental trials and is likely to be caused by bias in the needle wires and by vertical misalignment of the gelatin cart and the actuation unit. Therefore, the results of Experiment 1 only show relative slip between single and paired actuation and cannot be used to quantify the absolute slip in our system.

Furthermore, because we used a feed-forward controller for the motors of the actuation unit, it is possible that some of the slip was due to a discrepancy between the desired and actual travel distance of the sliders in the transmission housing. Lastly, the inertia of the gelatin cart influences the slip in both the pushing and the pulling phases. In the pushing phase a large gelatin mass is favorable for reducing slip, whereas in the pulling phase the contrary holds. Because of this influence of the gelatin cart, only qualitative conclusions regarding the slip can be drawn.

2) *Experiment 2:* The undesired upward deflection of the needle described in the previous paragraph also distorts the steering curvature results. For this reason the absolute steering curvature could not be determined.

Furthermore, the aforementioned directional bias observed in our steering experiment only allows for a qualitative comparison between steering conditions.

D. Future Work

Several design improvements in the needle prototype as well as in the actuation unit and the test rig should be implemented in future work. First, the glue connection between the aluminium interlocking ring and the central wire (NiTi) had to be renewed several times during Experiment 1 & 2. Replacing the NiTi central wire with a thinner stainless steel wire matching the flexibility of the NiTi wire would potentially result in a stronger and more reliable glue connection. Moreover, the design of the actuation unit should be improved to achieve higher accuracy and reliability when moving the needle wires. Specifically, the positioning accuracy of the leadscrew slider mechanism could be improved by adding a feedback loop in which the position of the sliders is monitored. The reliability

of this transmission mechanism would likely benefit from using rolling friction between the sliders and the transmission housing instead of sliding friction.

Removing the steering bias to the right as well as the undesired upward deflection of the needle during insertion would improve the quality of the results as pointed out before. First steps toward this goal could be to use wires that are less curved when relaxed than the current ones. Further, the bearing arrangement of the gelatin cart wheels should be redesigned in such a way that lateral motion of the gelatin caused by pivoting of the cart about the wheel bearings is eliminated. Accurate vertical alignment of the actuation unit and gelatin cart should be ensured by, for example, decreasing manufacturing and assembly tolerances. The experimental quantification of the slip during forward motion of the needle would benefit from eliminating the inertia effects of the gelatin cart. To do so, the viability of continuous needle insertion at constant speed instead of discrete insertion as presently utilized should be investigated.

To further improve the needle concept bifurcation of the needle segments has to be prevented. An interlocking ring in which neighboring needle segments touch each other could be a first step toward this. Measuring the cutting and friction forces of the needle wires and interlocking ring is necessary to gain a better understanding into the number needle segments that is required for moving the needle forward without slip. This becomes particularly relevant when a stiffer gelatin (or other substrate) is used since slip during the forward motion of a non-textured multi-segmented needle was found to be proportional to gelatin stiffness [31]. Better knowledge of the friction and cutting forces as well as their dependency on the gelatin stiffness would help determining the maximum gelatin stiffness for which a needle constructed of non-textured wires is feasible.

In order to find the optimal number of needle segments for a given application, future work should be directed toward the optimization problem mentioned in section II-B. In doing so, the relation between the number of needle segments and needle deflection as well as slip during forward motion should first be established analytically or experimentally followed by the formulation of a suitable cost function.

Note that the six-segmented needle presented and evaluated in this study represents only one of the many possible needle designs originating from our steerable needle concept. Apart from the advantages that a needle with a different number of movable segments might bring, multi-material as well as differing segment size designs could prove advantageous for applications in which a specific steering direction is desired.

Considering its intended use in the operating room a multi-segmented needle poses challenges to the cleaning of such an instrument. Cleaning methods or design for single-use should be considered in the following design iterations. The current needle concept does not feature a channel for the delivery or collection of substances. Possibilities to replace one (or more) of the wires by a flexible tube should be investigated.

Future work should also expand on the experimental characterization of the present study by investigating variables such as insertion speed, gelatin stiffness and actuation pattern.

Data acquisition at a higher sampling rate would allow insight into the acceleration of the gelatin cart during pushing and pulling phase. This insight could potentially help to quantify the influence of the inertia of the gelatin cart on the slip of the needle. Moreover, an experimental setup with two cameras positioned perpendicular to each other would allow for a 3D steering analysis of the needle.

VII. CONCLUSION

By expanding on the anatomy and working principle of wasp ovipositors we have developed a novel approach for the design of steerable needles that can penetrate tissue with zero axial push force and steering in 3D without axial rotation of the needle while being small enough to be used in core-needle biopsy and brachytherapy procedures. Based on this approach, a needle research prototype with a diameter of 1.2 mm was developed and experimentally evaluated. It was found that the slip during forward motion of our needle prototype is less than in a previous non-textured needle prototype. Furthermore, steering by means of a ‘quasi’ bevel-tip proved viable, allowing for steering curvatures as high as 0.0184 1/cm. However, the bias in the NiTi wires used as needle segments as well as bifurcation of the wires when pushed inside the gelatin limit the conclusiveness of our steering experiments. For this reason modifications to the experimental setup and the needle followed by a re-evaluation of the steering performance of the needle prototype are recommended for future work.

ACKNOWLEDGMENTS

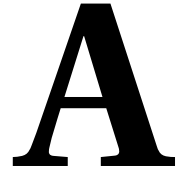
The author would like to thank Menno Lageweg, David Jager and Danny de Gans from DEMO (Dienst Elektronische en Mechanische Ontwikkeling at TU Delft) for fabricating the needle prototype and their help with the electronic system design.

REFERENCES

- [1] Youk, J. H., Kim, E. K., Kim, M. J., Kwak, J. Y., & Son, E. J. (2010). Analysis of false-negative results after US-guided 14-gauge core needle breast biopsy. *European Radiology*, 20(4), 782-789.
- [2] Volpe, A., Kachura, J. R., Geddie, W. R., Evans, A. J., Gharajeh, A., Saravanan, A., & Jewett, M. A. (2007). Techniques, safety and accuracy of sampling of renal tumors by fine needle aspiration and core biopsy. *The Journal of Urology*, 178(2), 379-386.
- [3] Wan, G., Wei, Z., Gardi, L., Downey, D. B., & Fenster, A. (2005). Brachytherapy needle deflection evaluation and correction. *Medical Physics*, 32(4), 902-909.
- [4] Jeng C. L., Torillo T. M., & Rosenblatt M. A. (2010). Complications of peripheral nerve blocks. *British Journal of Anaesthesia*, 105(suppl 1): i97-i107.
- [5] Eapen, L., Kayser, C., Deshaies, Y., Perry, G., Choan, E., Morash, C., ... & Dahrouge, S. (2004). Correlating the degree of needle trauma during prostate brachytherapy and the development of acute urinary toxicity. *International Journal of Radiation Oncology* Biology* Physics*, 59(5), 1392-1394.
- [6] Stone, N. N., Roy, J., Hong, S., Lo, Y. C., & Stock, R. G. (2002). Prostate gland motion and deformation caused by needle placement during brachytherapy. *Brachytherapy*, 1(3), 154-160.
- [7] Kohn, L. T., Corrigan, J. M., & Donaldson, M. S. (Eds.). (2000). *To err is human:: building a safer health system* (Vol. 6). National Academies Press.

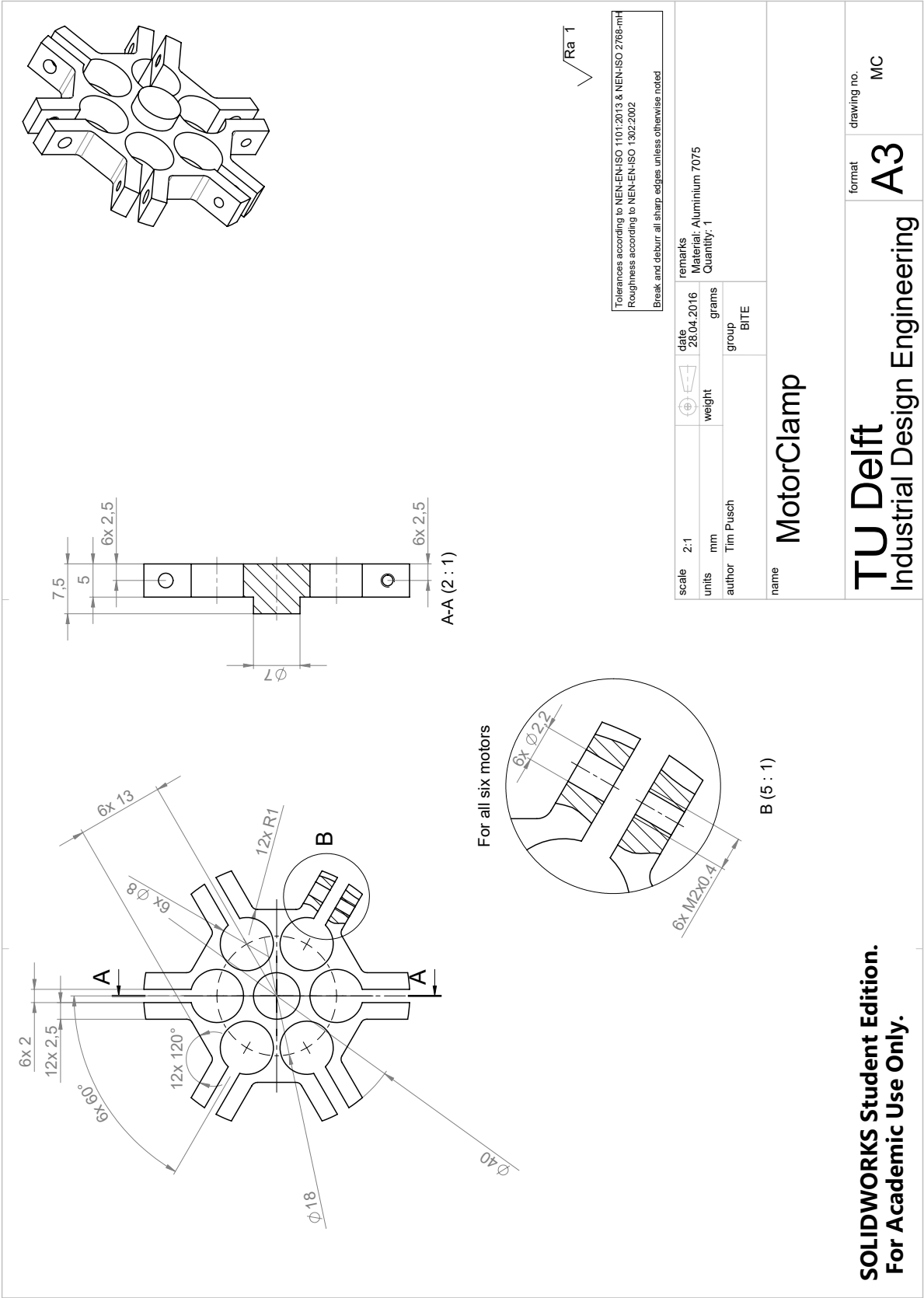
- [8] Carr, J. J., Hemler, P. F., Halford, P. W., Freimanis, R. I., Choplin, R. H., & Chen, M. Y. (2001). Stereotactic localization of breast lesions: how it works and methods to improve accuracy. *Radiographics*, 21(2), 463-473.
- [9] Podder, T. K., Dicker, A. P., Hutapea, P., Darvish, K., & Yu, Y. (2012). A novel curvilinear approach for prostate seed implantation. *Medical Physics*, 39(4), 1887-1892.
- [10] Scali M., Pusch T. P., Breedveld P. & Dodou D. (2016). Needle-like instruments for steering through solid organs: a review of the scientific and patent literature. [Paper submitted for publication].
- [11] Abolhassani, N., Patel, R., & Moallem, M. (2007). Needle insertion into soft tissue: a survey. *Medical Engineering & Physics*, 29(4), 413-431.
- [12] Cowan, N. J., Goldberg, K., Chirikjian, G. S., Fichtinger, G., Alterovitz, R., Reed, K. B., ... & Okamura, A. M. (2011). Robotic needle steering: design, modeling, planning, and image guidance. *Surgical Robotics* (pp. 557-582). Springer US.
- [13] van de Berg, N. J., van Gerwen, D. J., Dankelman, J., & van den Dobbelsteen, J. J. (2015). Design choices in needle steering - a review. *IEEE/ASME Transactions on Mechatronics*, 20(5), 2172-2183.
- [14] Swaney, P. J., Burgner, J., Gilbert, H. B., & Webster, R. J. (2013). A flexure-based steerable needle: high curvature with reduced tissue damage. *IEEE Transactions on Biomedical Engineering*, 60(4), 906-909.
- [15] Wang, Y. Z., Yin, Q. L., Liu, C. J., & Chen, Y. H. (2012). Towards an articulated needle. In *Applied Mechanics and Materials* (Vol. 152, pp. 946-951). Trans Tech Publications.
- [16] Okazawa, S., Ebrahimi, R., Chuang, J., Salcudean, S. E., & Rohling, R. (2005). Hand-held steerable needle device. *IEEE/ASME Transactions on Mechatronics*, 10(3), 285-296.
- [17] Webster III, R. J., Okamura, A. M., & Cowan, N. J. (2006). Toward active cannulas: Miniature snake-like surgical robots. In *2006 IEEE/RSJ International Conference on Intelligent Robots and Systems* (pp. 2857-2863). IEEE.
- [18] van de Berg, N. J., Dankelman, J., & van den Dobbelsteen, J. J. (2015). Design of an actively controlled steerable needle with tendon actuation and FBG-based shape sensing. *Medical Engineering & Physics* 37(6), 617-622.
- [19] Losey, D. P., York, P. A., Swaney, P. J., Burgner, J., & Webster, R. J. (2013). A flexure-based wrist for needle-sized surgical robots. In *SPIE Medical Imaging*, 86711G. International Society of Optics and Photonics.
- [20] Reed, K. B., Majewicz, A., Kallem, V., Alterovitz, R., Goldberg, K., Cowan, N. J., & Okamura, A. M. (2011). Robot-assisted needle steering. *Robotics & Automation Magazine, IEEE*, 18(4), 35-46.
- [21] Swensen, J. P., Lin, M., Okamura, A. M., & Cowan, N. J. (2014). Torsional dynamics of steerable needles: modeling and fluoroscopic guidance. *IEEE Transactions on Biomedical Engineering*, 61(11), 2707-2717.
- [22] Reed, K. B., Okamura, A. M., & Cowan, N. J. (2009). Modeling and control of needles with torsional friction. *IEEE Transactions on Biomedical Engineering*, 56(12), 2905-2916.
- [23] Quicke, D. L. J., Fitton, M. G., Tunstead, J. R., Ingram, S. N., & Gaitens, P. V. (1994). Ovipositor structure and relationships within the Hymenoptera, with special reference to the Ichneumonidea. *Journal of Natural History*, 28(3), 635-682.
- [24] Vincent, J. F. V., & King, M. J. (1995). The mechanism of drilling by wood wasp ovipositors. *Biomimetics (USA)*.
- [25] Sakes, A., Dodou, D., & Breedveld, P. (2016). Buckling prevention strategies in nature as inspiration for improving percutaneous instruments: a review. *Bioinspiration & Biomimetics*, 11(2), 021001.
- [26] Quicke, D. L. J., Fitton, M. G., & Harris, J. (1995). Ovipositor steering mechanisms in braconid wasps. *Journal of Hymenoptera Research*, 4, 110-120.
- [27] Quicke, D. L. J. (1991). Ovipositor mechanics of the braconine wasp genus *Zaglyptogastra* and the ichneumonid genus *Pristomerus*. *Journal of Natural History*, 25(4), 971-977.
- [28] Gouache, T., Coste, P., Gao, Y., & Gourinat, Y. (2010). *Wood wasp inspired planetary and Earth drill*. INTECH Open Access Publisher.
- [29] Nakajima, K. & Schwarz O. (2014). How to use the ovipositor drilling mechanism of Hymenoptera for developing a surgical instrument in biomimetic design. *International Journal of Design & Nature and Ecodynamics*, 9(3), 177189.
- [30] Frasson, L., Ko, S. Y., Turner, A., Parittotokkaporn, T., Vincent, J. F., & Rodriguez y Baena, F. (2010). STING: a soft-tissue intervention and neurosurgical guide to access deep brain lesions through curved trajectories. *Proceedings of the Institution of Mechanical Engineers, Part H: Journal of Engineering in Medicine*, 224(6), 775-788.
- [31] Sprang, T. (2014). *Ovipositor-inspired needle insertion without a net push force* (Master's thesis). Retrieved from TU Delft Repository. (Accession Order No. uuid:35298358-6104-4bc8-95ab-cab897755489)
- [32] Oldfield, M. J., Leibinger, A., Seah, T. E. T., & Rodriguez y Baena, F. (2015). Method to reduce target motion through needletissue interactions. *Annals of Biomedical Engineering*, 43(11), 2794-2803.
- [33] Oldfield, M. J., Burrows, C., Kerl, J., Frasson, L., Parittotokkaporn, T., Beyrau, F., & Rodriguez y Baena, F. (2014). Highly resolved strain imaging during needle insertion: results with a novel biologically inspired device. *Journal of the Mechanical Behavior of Biomedical Materials*, 30, 50-60.
- [34] Leibinger, A., Oldfield, M., & Rodriguez y Baena, F. (2014). Multi-objective design optimization of a steerable needle for soft tissue surgery. In *The 15th International Conference on Biomedical Engineering* (pp. 420-423). Springer International Publishing.
- [35] Frasson, L., Reina, S., Davies, B. L., & Rodriguez y Baena, F. (2009). Design optimization of a biologically inspired multi-part probe for soft tissue surgery. In *World Congress on Medical Physics and Biomedical Engineering, September 7-12, 2009, Munich, Germany* (pp. 307-310). Springer Berlin Heidelberg.
- [36] Ko, S. Y., & Frasson, L. (2011). Closed-loop planar motion control of a steerable probe with a "programmable bevel" inspired by nature. *IEEE Transactions on Robotics*, 27(5), 970-983.
- [37] Ko, S. Y., & Rodriguez y Baena, F. (2013). Toward a miniaturized needle steering system with path planning for obstacle avoidance. *IEEE Transactions on Biomedical Engineering*, 60(4), 910-917.
- [38] Frasson, L., Ferroni, F., Ko, S. Y., Dogangil, G., & Rodriguez y Baena, F. (2012). Experimental evaluation of a novel steerable probe with a programmable bevel tip inspired by nature. *Journal of Robotic Surgery*, 6(3), 189-197.
- [39] Webster III, R. J., Memisevic, J., & Okamura, A. M. (2005). Design considerations for robotic needle steering. In *Proceedings of the 2005 IEEE International Conference on Robotics and Automation (ICRA)* (pp. 3588-3594). IEEE.
- [40] Misra, S., Reed, K. B., Schafer, B. W., Ramesh, K. T., & Okamura, A. M. (2010). Mechanics of flexible needles robotically steered through soft tissue. *The International Journal of Robotics Research*, 29(13), 1640-1660.
- [41] Gheradi, G. (2010). *Fine-needle biopsy of superficial and deep masses: interventional approach and interpretation methodology by pattern recognition*. Springer Science & Business Media.
- [42] Bard Medical, *FASTFILL Brachytherapy Needle*. Retrieved from <http://www.bardmedical.com/products/prostate-health/brachytherapy/needles/> [Accessed 15 April 2016].
- [43] Cook Medical, *Cook Brachytherapy Needle*. Retrieved from https://www.cookmedical.com/products/uro_cbn_webds/ [Accessed 15 April 2016].
- [44] Hing, J. T., Brooks, A. D., & Desai, J. P. (2006). Reality-based needle insertion simulation for haptic feedback in prostate brachytherapy. In *Proceedings of the 2006 IEEE International Conference on Robotics and Automation (ICRA)* (pp. 619-624). IEEE.
- [45] Parittotokkaporn, T., Frasson, L., Schneider, A., Davies, B. L., De-genaar, P., & Rodriguez y Baena, F. (2010). Insertion experiments of a biologically inspired microtextured and multi-part probe based on reciprocal motion. In *Engineering in Medicine and Biology Society (EMBC), 2010 Annual International Conference of the IEEE* (pp. 3190-3193). IEEE.

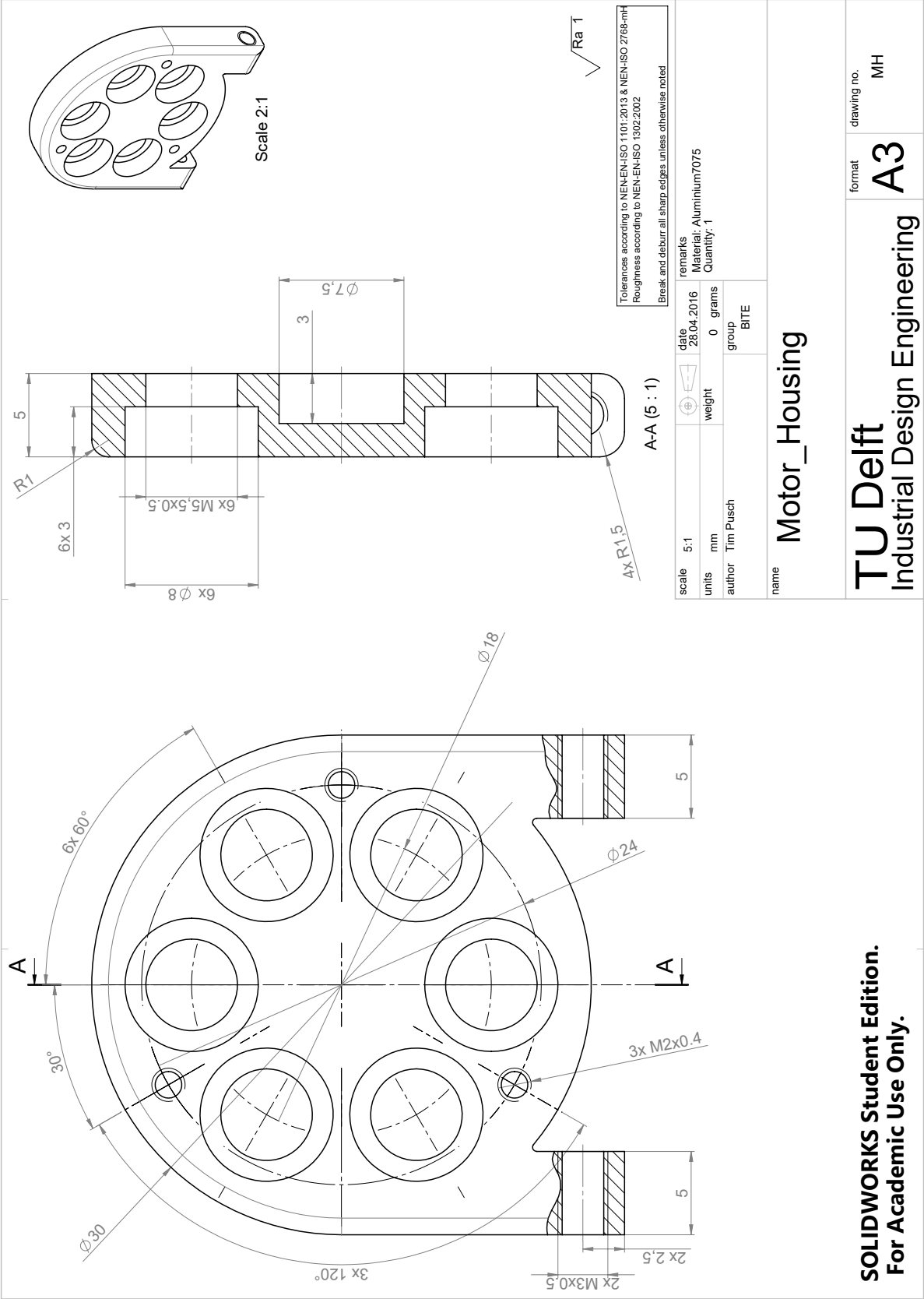
- [46] Burrows, C., Secoli, R., & Rodriguez y Baena, F. (2013). Experimental characterisation of a biologically inspired 3D steering needle. In *13th International Conference on Control, Automation and Systems (ICCAS)* (pp. 1252-1257). IEEE.
- [47] van Gerwen, D. J., Dankelman, J., & van den Dobbelsteen, J. J. (2012). Needle-tissue interaction forces – a survey of experimental data. *Medical Engineering & Physics*, 34(6), 665-680.
- [48] Kundanati, L., *Parasitic fig wasp Apocrypta westwoodi on a fig*. Retrieved from <http://www.sci-news.com/biology/science-fig-wasps-zinc-ovipositor-01951.html> [Accessed 05 Mai 2016].

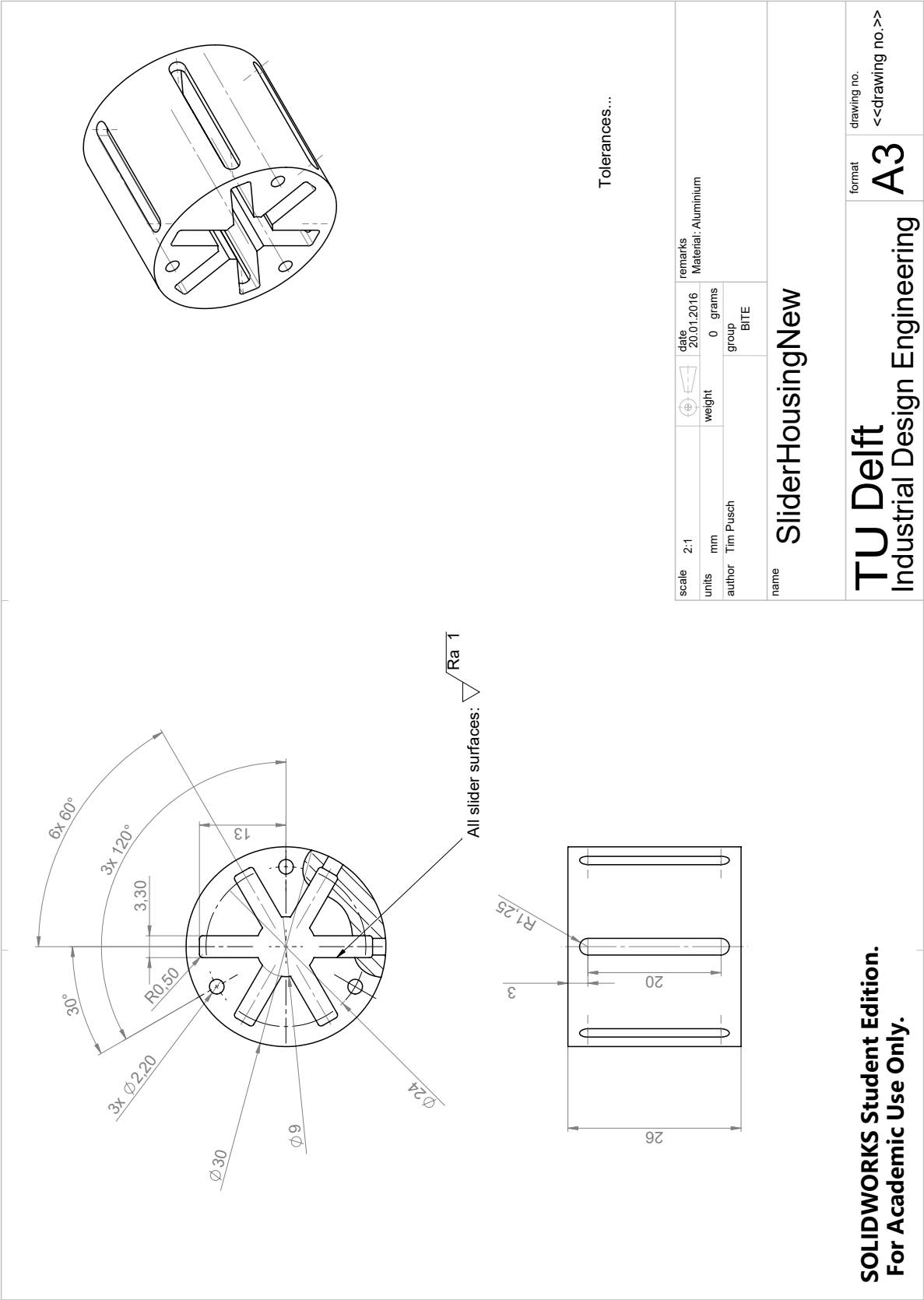


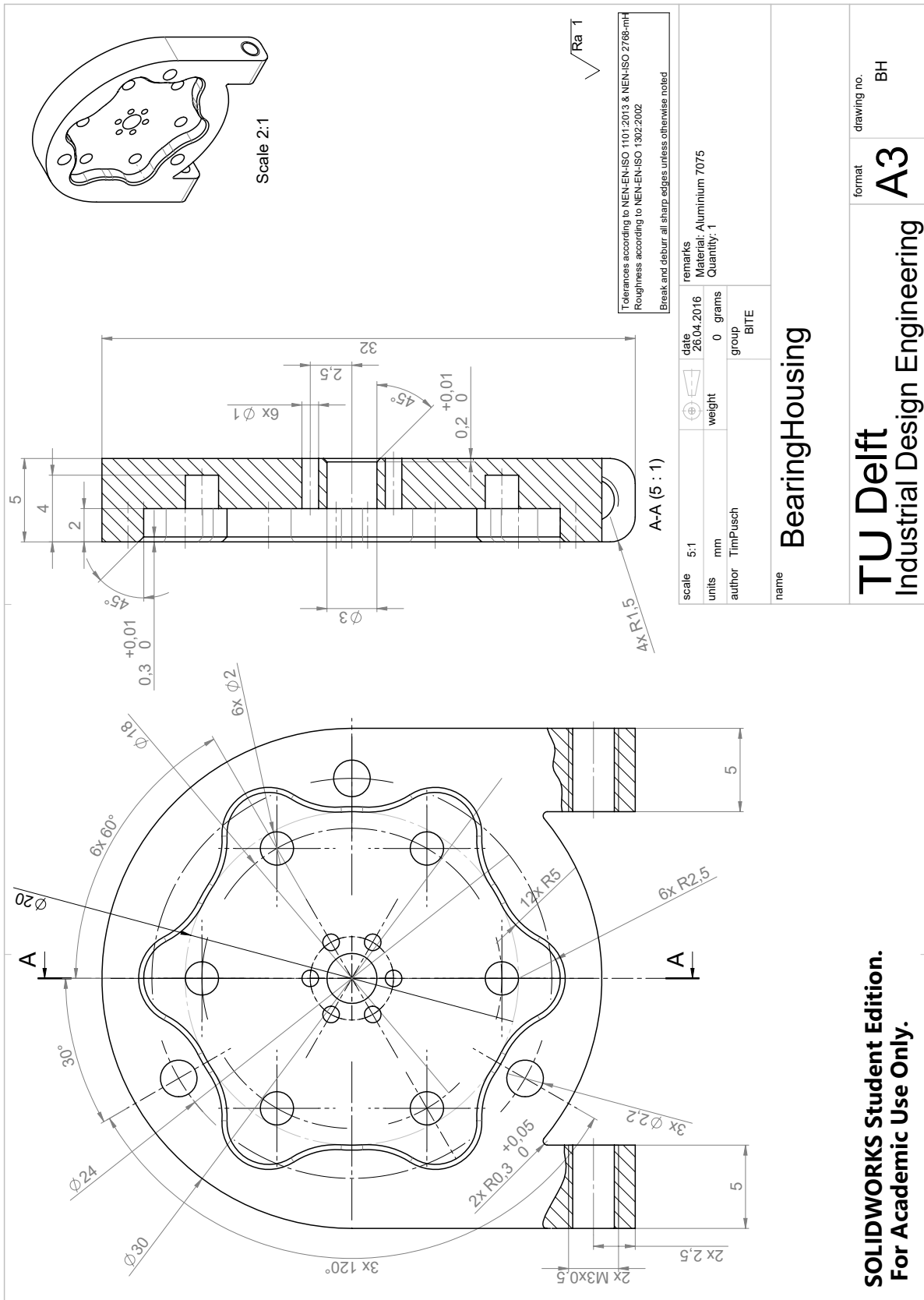
ENGINEERING DRAWINGS

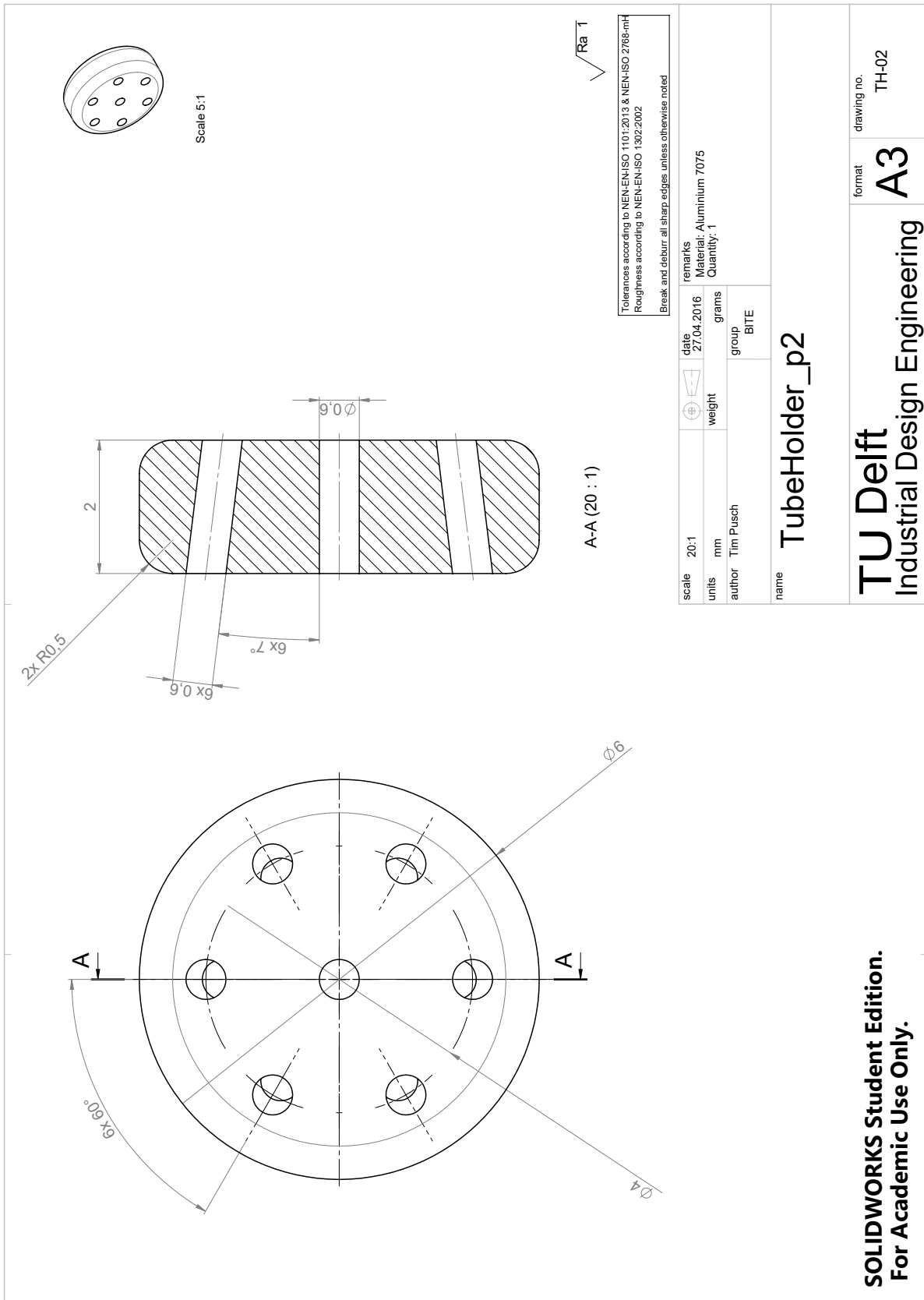
This appendix comprises the engineering drawings for the actuation unit as well as the drawings of the Alignment Ring and the Interlocking Ring. The assembly and cross section drawings of the actuation unit can be found in section III of the scientific paper.

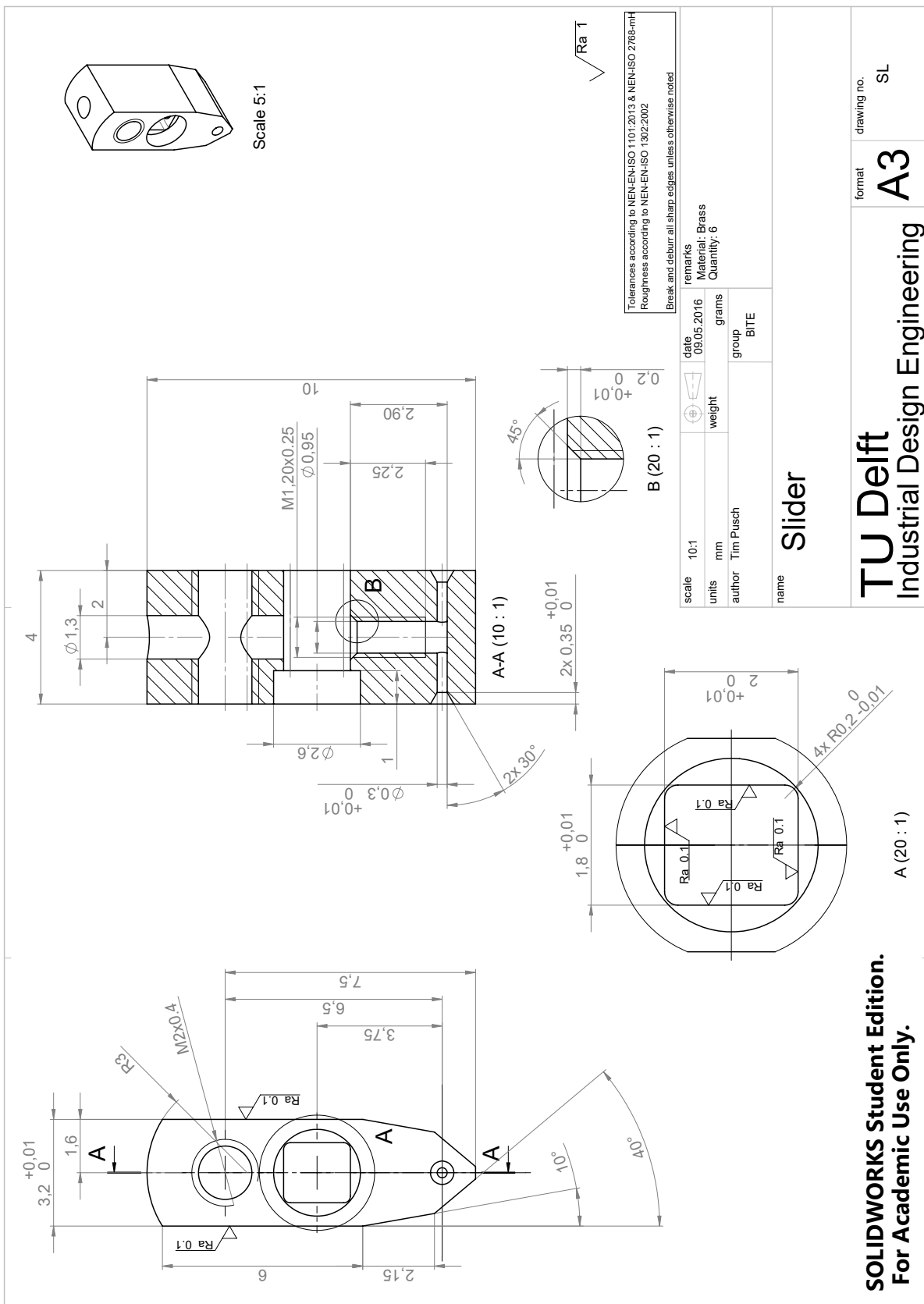


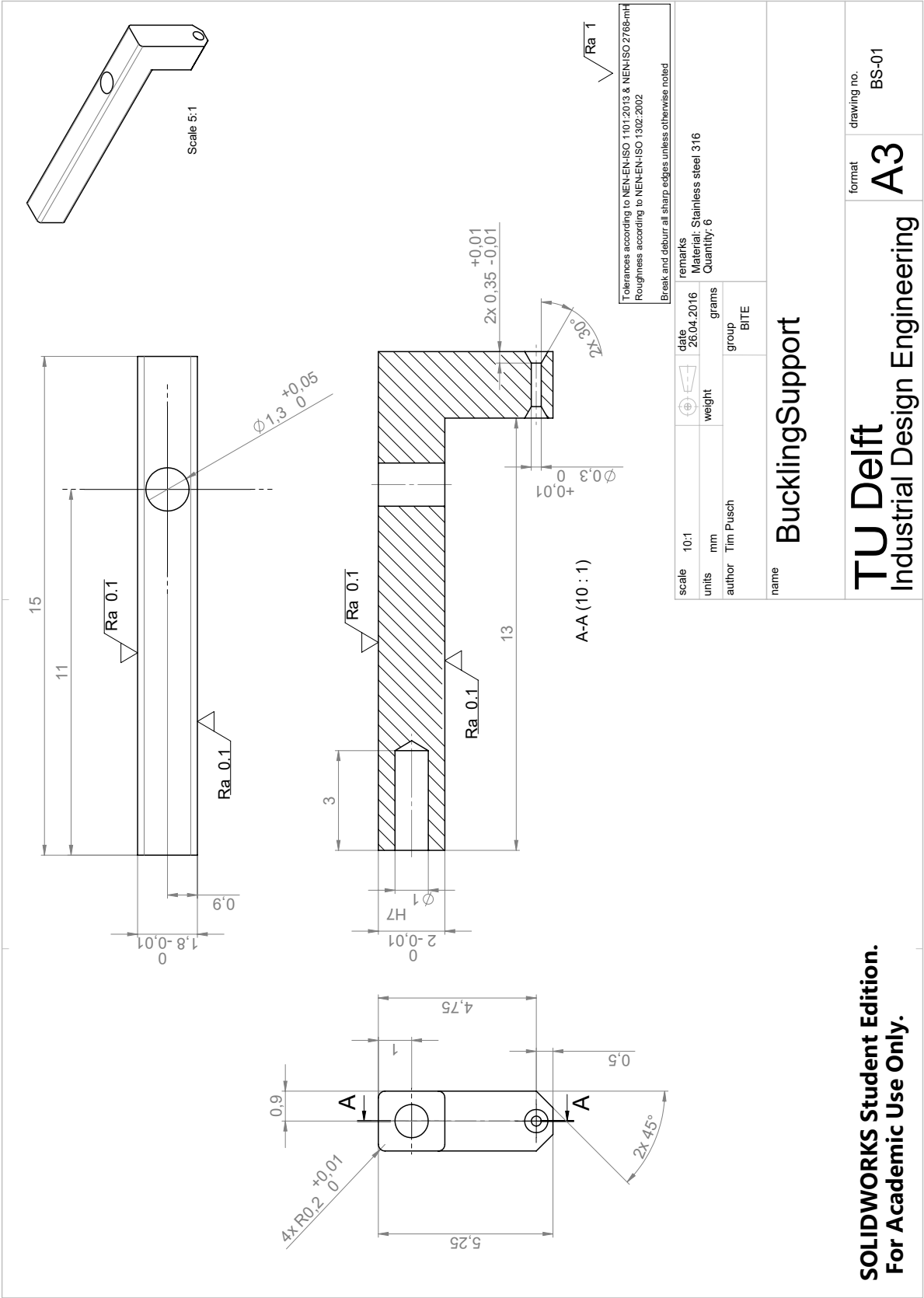


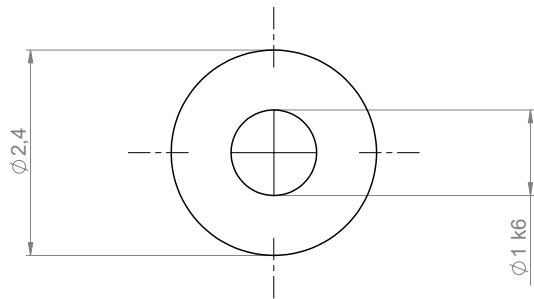












Scale 5:1

Ra 1

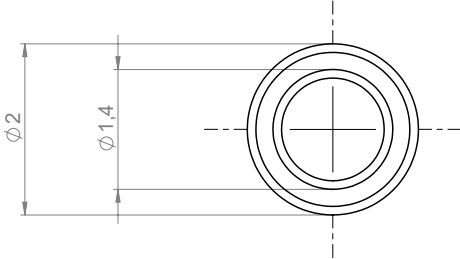
Tolerances according to NEN-EN-ISO 1101:2013 & NEN-ISO 2768-mH
Roughness according to NEN-EN-ISO 1302:2002

scale	20:1	weight	date	remarks
units	mm	grams		
author	Tim Pusch	group	BITE	Material: Stainless steel 316 Quantity: 6

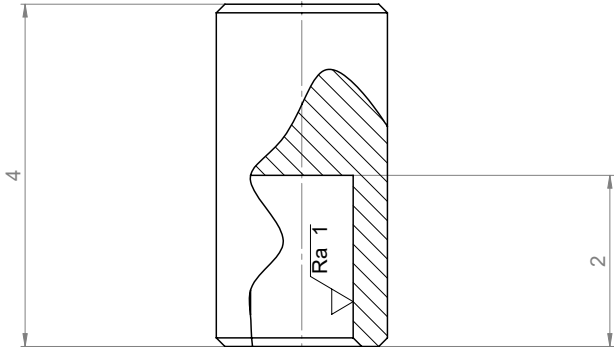
BucklingSupport_plugin

**SOLIDWORKS Student Edition.
For Academic Use Only.**

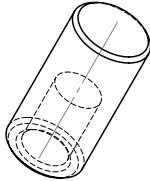
TU Delft Industrial Design Engineering	format A3	drawing no. BS-02
---	---------------------	----------------------



$\phi 2$
 $\phi 1,4$



4
2
Ra 1



Scale 10:1

All chamfers 45° x 0.1

scale

20:1

units

mm

author

Tim Pusch

weight

date

21.01.2016

group

BITE

grams

remarks

Material: Brass

name

SlidingBearing

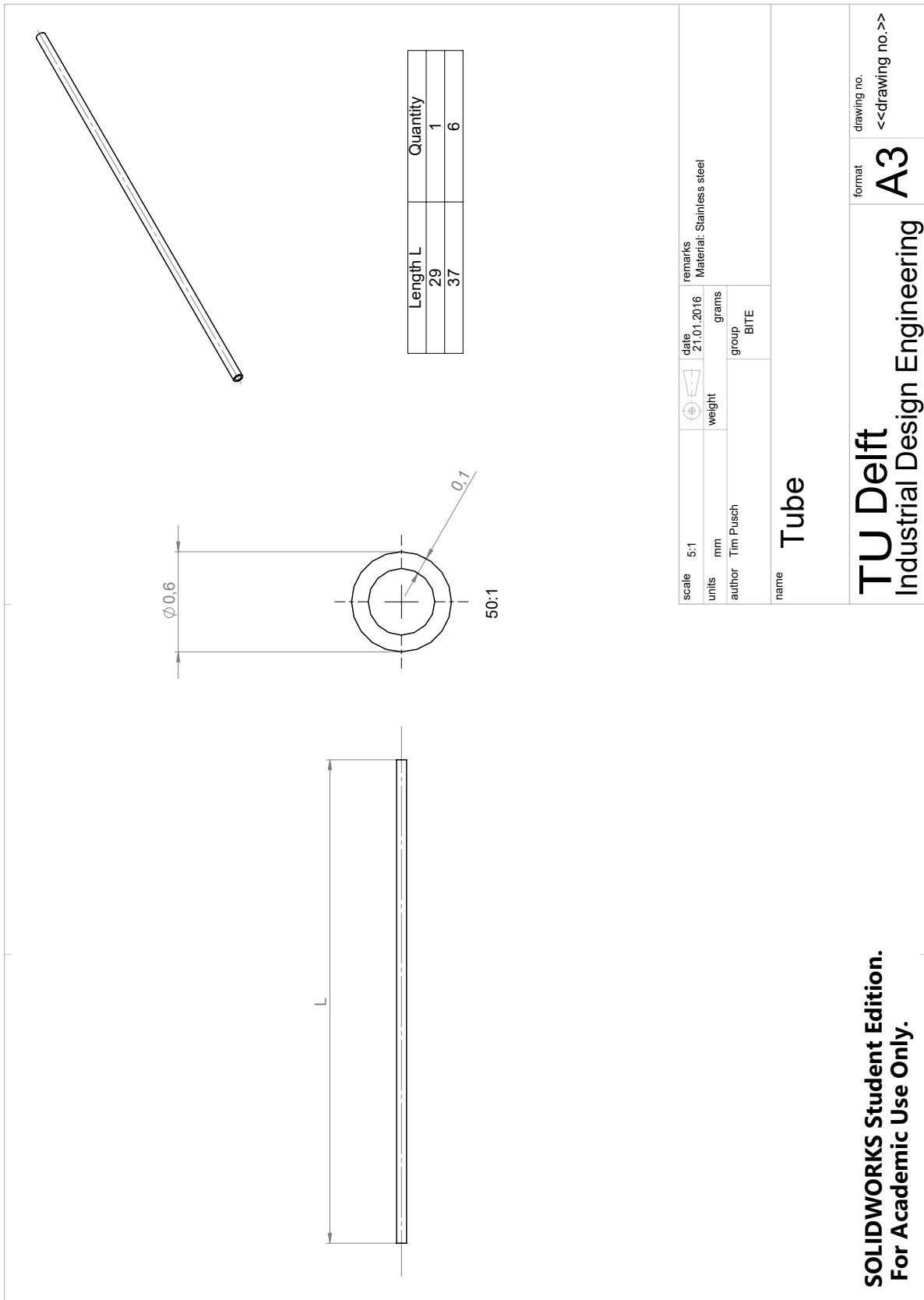
format

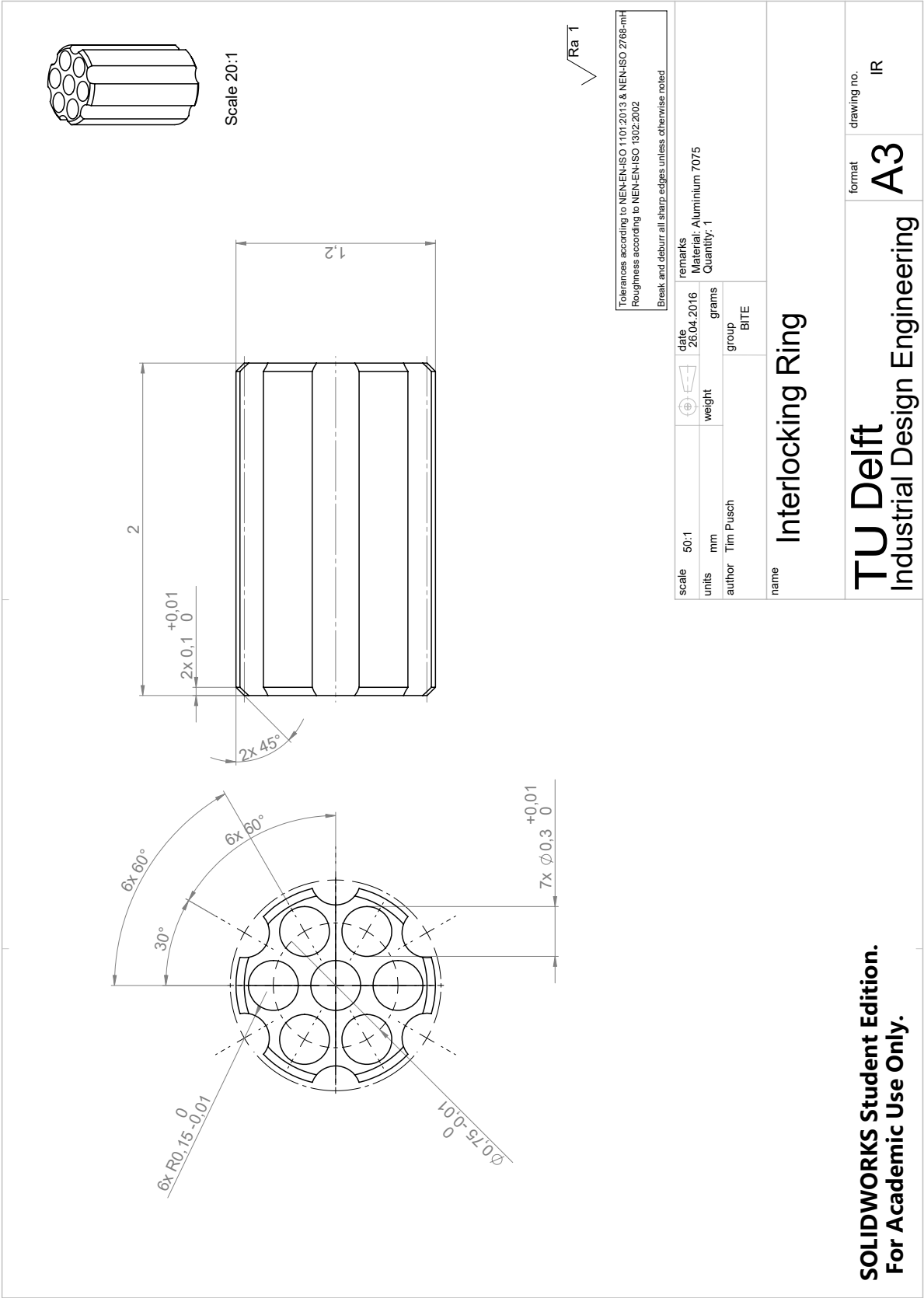
A3

drawing no.

<<drawing no.>>

SOLIDWORKS Student Edition.
For Academic Use Only.





B

ARDUINO CODE

This appendix contains the Arduino code written for performing Experiment 1 & 2. The general structure of the software is outlined in B.1. The software was divided into two parts: the main sketch and the `moveMotor` function. The main sketch is uploaded on the Arduino controller board and contains the structure of the software as shown in B.1. The `moveMotor` function takes inputs regarding motor to be used, speed, and travel distance as specified in the main sketch and makes the motors move accordingly. The `Ge1Stepper.h` library for translating the code information to electrical signals for the motors was provided by DEMO.

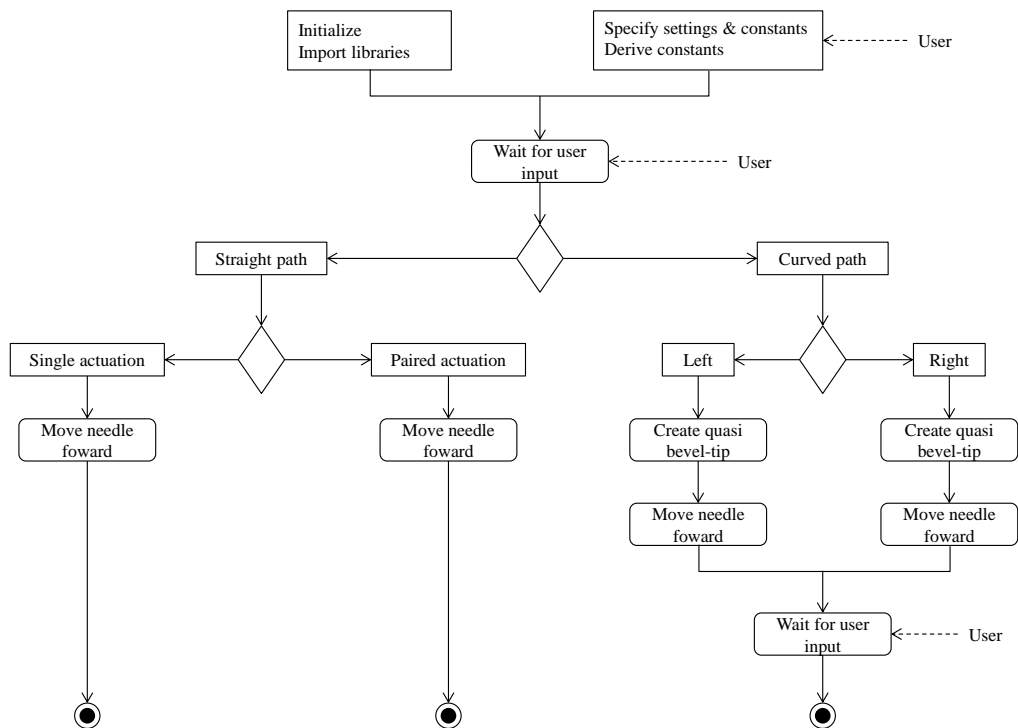


Figure B.1: Arduino IDE code schematic.

B.1. MAIN SKETCH

The trial settings (i.e., motor speed, bevel offset, dynamic offset, straight or steering mode, total travel distance, single or double actuation) can be specified at the top portion of the main sketch ('SETTINGS'). In the following portion of the code ('MOTORS'), the motor masks for actuating individual motors or a combination of multiple motors are created. The 'CONSTANTS' code portion contains operations for converting the specified value of the total travel distance and the travel speed to variables that can be used in the code.

Since the code is based on for-loops, the specified total travel distance ($TDIST$) was converted to the total number of cycles ($totNumCycles$). This total number of cycles was then used to specify how many times a for-loop was to be repeated. In one cycle all motors are first move forward individually (or pairwise) and then pulled back simultaneously. The total number of cycles was calculated as

$$totNumCycles = \frac{TDIST}{mOffset}, \quad (B.1)$$

where $mOffset$ represents the dynamic offset. The $\text{ceil}()$ operator was used in the code to round $totNumCycles$ up to the next higher integer if the calculation yielded a decimal number.

The travel speed specified in SETTINGS had to be converted to a delay value to be of use when sending electrical signals to the stepper motors. Two times the delay value corresponds to the time it takes for the stepper motor to take one step. The delay could thus be calculated as:

$$delay = \frac{p}{2 \cdot s_r \cdot v} [\mu s], \quad (B.2)$$

where p is the leadscrew pitch (i.e., 0.2 mm), s_r the number of steps the motor has to take for one revolution in the selected mode (i.e., 20 in full-step mode), and v the desired travel speed of the needle wire. In the code, the $\text{round}()$ operator was used to ensure $delay$ was rounded to the closest integer if necessary.

When running the code, the user is first prompted to start the trial by entering 'ok' in the Arduino serial monitor. After this command has been given, the program executes the trial according to the specified settings.

```

//This is the main sketch for actuating the needle.

////////////////////////////////////
////////////////////////////////////  INITIALIZATION  //////////////////////////////////
////////////////////////////////////

// SETUP.

#include <GelStepper.h> //include GelStepper library to main file
GelStepper GS; // initialize GelStepper

#include <math.h> //include math library

#include "moveMotor.h" //include moveMotor header function to main file

//-----
//-----USER INPUT-----
//-----
// SETTINGS. This section specifies the parameter levels (such as speed, offset, bevel angle),
// actuation mode settings (such as straight/curved, single/double). The variables listed in this
// section have to be set to the desired value (or mode) for each experiment.

float mSpeed = 2.0; //desired travel speed of selected motor in [mm/s]. Change to desired value.
float mOffset = 4.0; //desired protrusion offset for each motor in [mm]. Change to desired value.
float bevOffset = 2.0; //desired bevel angle offset in [mm]. Change to desired value.
String motionMode = "straight"; //desired motion mode setting for needle path. Select either
'straight' or 'curved'.
String actMode = "sing"; //desired actuation mode setting for straight needle path. Select either
'sing' (single) or 'doub' (double).
String dir = "left"; //desired steering direction if motion mode is "curved". Select either 'left'
or 'right'.
int TDIST = 120; //total travel distance of gel-cart in [mm]

//-----

// MOTORS. Binary masks for stepping individual/or combination of several motors.

unsigned char mot1 = B00000001; //mask for motor 1
unsigned char mot2 = B00000010; //mask for motor 2
unsigned char mot3 = B00000100; //mask for motor 3
unsigned char mot4 = B00001000; //mask for motor 4
unsigned char mot5 = B00010000; //mask for motor 5
unsigned char mot6 = B00100000; //mask for motor 6
unsigned char mot12 = B00000011; //mask for motor 1&2
unsigned char mot16 = B00100001; //mask for motor 1&6
unsigned char mot23 = B00000110; //mask for motor 2&3
unsigned char mot34 = B00001100; //mask for motor 3&4
unsigned char mot45 = B00011000; //mask for motor 4&5
unsigned char mot56 = B00110000; //mask for motor 5&6
unsigned char motAll = B00111111; //mask for motor 1-6
unsigned char motBev1; //initialize mask
unsigned char motBev2; //initialize mask
unsigned char motPair1; //initialize mask
unsigned char motPair2; //initialize mask
unsigned char motPair3; //initialize mask

// DERIVED CONSTANTS (SPECIFIED AND DERIVED). All the necessary constants are specified here.

boolean state = true; //'state' is toggled at the end of void loop() function to make sure it only
runs once.
String stateCheck; //String variable that let's user start the program manually.

int totNumCycles = ceil(TDIST / mOffset); //number of cycles. derived from total travel distance
and desired protrusion offset. Is rounded up to the next integer.
int mDelay = round((0.2*1000000)/(mSpeed*2*20)); //time delay [us] derived from desired travel
speed. formula: LeadScrewPitch/(speed*2*stepsPerRev). stepsPerRev depends on step settings of motor
(full step mode: 20 steps for one rev.)

int ii = 1; //counter for void loop function

```

```

////////////////////////////////////
////////////////////////////////////  START  //////////////////////////////////
////////////////////////////////////

void setup() {

  // Full step: M0,0 & M1,0
  // Half step: M0,1 & M1,0
  // 1/4 step: M0,floating & M1,0
  // 1/8 step: M0,0 & M1,1
  // 1/16 step: M0,1 & M1,1
  // 1/32 step: M0,floating & M1,1

  digitalWrite(M0,0); // pin M0 for all 6 motors
  digitalWrite(M1,0); // pin M1 for all 6 motors
  digitalWrite(EN,0); // nEN for all 6 motors
  digitalWrite(SLPCFG,1); // combined nSLEEP and CONFIG pins for all 6 motors

  Serial.begin(9600); //opens serial port at 9600bps.

}

void loop() {

  // determine motor sequence for curved trajectory
  if(dir == "left"){
    motBev1 = mot5;
    motBev2 = mot6;
    motPair1 = mot16;
    motPair2 = mot45;
    motPair3 = mot23;
  }

  else if(dir == "right"){
    motBev1 = mot2;
    motBev2 = mot3;
    motPair1 = mot12;
    motPair2 = mot34;
    motPair3 = mot56;
  }

  else{
    ii = 2;
  }

  Serial.println("Enter 'ok' to start the program...");
  while(Serial.available()==0){ //empty while loop to wait for user input.
  }

  stateCheck = Serial.readString(); //reads user input.

  if(ii == 1 && stateCheck=="ok" || stateCheck=="Ok" || stateCheck=="OK"){ //if input is
'ok', state is toggled to 'true' and program starts.
    state = true;
  }

  else{
    state = false; //any input other than 'ok' will run void loop() w/o doing anything.
  }

  if(state == true) //this if statement makes sure void loop() does not continue running.
  {
    Serial.println("Program started...");

    if(motionMode == "straight") //straight path
    {

      if(actMode == "sing") //single actuation mode.
      {

```



```

    for(int numCycles = 0; numCycles <= totNumCycles-1; numCycles++) //iterate for entire
travel distance.
    {
        DIR.COMBINED.MOTORS = 0; //set direction pins forward. equal to B000000.

        moveMotor(mot1, mDelay, mOffset); //call moveMotor function for motor 1
        moveMotor(mot2, mDelay, mOffset); //call moveMotor function for motor 2
        moveMotor(mot3, mDelay, mOffset); //call moveMotor function for motor 3
        moveMotor(mot4, mDelay, mOffset); //call moveMotor function for motor 4
        moveMotor(mot5, mDelay, mOffset); //call moveMotor function for motor 5
        moveMotor(mot6, mDelay, mOffset); //call moveMotor function for motor 6

        DIR.COMBINED.MOTORS = ~DIR.COMBINED.MOTORS; //reverse direction.

        moveMotor(motAll, mDelay, mOffset); //call moveMotor function for motor 1-6

        Serial.println(numCycles+1); //shows number of cycles on serial monitor
    }
}

else if(actMode == "doub") //double actuation mode.
{
    for(int numCycles = 0; numCycles <= totNumCycles-1; numCycles++) //iterate for entire
travel distance.
    {
        DIR.COMBINED.MOTORS = 0; //set direction pins forward. equal to B000000.

        moveMotor(mot12, mDelay, mOffset); //call moveMotor function for motor 1 & 2
        moveMotor(mot34, mDelay, mOffset); //call moveMotor function for motor 3 & 4
        moveMotor(mot56, mDelay, mOffset); //call moveMotor function for motor 5 & 6

        DIR.COMBINED.MOTORS = ~DIR.COMBINED.MOTORS; //reverse direction.

        moveMotor(motAll, mDelay, mOffset); //call moveMotor function for motor 1-6
    }
}

else
{
    Serial.println("Unknown actuation mode specified. Choose between 'sing' and 'doub'.");
}
} //closes motionMode="straight" if-statement

else if(motionMode == "curved")
{
    DIR.COMBINED.MOTORS = 0; //set direction pins forward. equal to B000000.

    moveMotor(motBev1, mDelay, bevOffset); //create bevel angle offset between wire 1 & 2 by
moving motor 2 (moves needle to the left)
    moveMotor(motBev2, mDelay, bevOffset); //create bevel angle offset between wire 3 & 4 by
moving motor 3 (moves needle to the left)

    for(int numCycles = 0; numCycles <= totNumCycles-1; numCycles++) //iterate for entire travel
distance.
    {
        DIR.COMBINED.MOTORS = 0; //set direction pins forward. equal to B000000.

        moveMotor(motPair1, mDelay, mOffset); //call moveMotor function for motor 1 & 2
        moveMotor(motPair2, mDelay, mOffset); //call moveMotor function for motor 3 & 4
        moveMotor(motPair3, mDelay, mOffset); //call moveMotor function for motor 5 & 6

        DIR.COMBINED.MOTORS = ~DIR.COMBINED.MOTORS; //reverse direction.

        moveMotor(motAll, mDelay, mOffset); //call moveMotor function for motor 1-6
    }

    Serial.println("Take picture. Enter 'done' to continue...");
}

```

```

        while(Serial.available()==0){    //empty while loop to wait for user
input.
        }

        String picCheck = Serial.readString(); //reads user input.

        if(picCheck == "done")
        {
            Serial.println("Resetting bevel...");
            DIR.COMBINED.MOTORS = 0x3F; //set direction pins backward. equal to B111111.

            moveMotor(motBev1, mDelay, bevOffset); //reset bevel angle offset between wire 1 & 2 by
moving motor 2
            moveMotor(motBev2, mDelay, bevOffset); //reset bevel angle offset between wire 3 & 4 by
moving motor 3
        }

        else
        {
            Serial.println("Continue without resetting bevel...");
        }

    }    //closes motionMode="curved" if-statement

    else
    {
        Serial.println("Unknown motion mode specified. Choose between 'straight' and 'curved'.");
    }
}    //closes state check if-statement

state = false; //toggle to 'false' to end void loop() function.
ii++; //counter + 1
Serial.println("The end.");
} //void loop end

```

B.2. MOVEMOTOR FUNCTION

The `moveMotor` function is responsible for making the motors take a step. It was set up in such a way that it receives information about the motor to be used (`motorMask`), the speed at which the motor is to run (derived from `mDelay`) and the number of steps the motor is supposed to take (calculated from `mOffset`) as the function input. The number of steps (*numSteps*) corresponds to the distance the actuated needle wire(s) is to be moved forward or backward by the motor(s). *numSteps* was calculated as

$$numSteps = \frac{r_s \cdot mOffset}{p}, \quad (B.3)$$

where r_s is the number of steps the motor has to take for one revolution in the selected mode (i.e., 20 in full-step mode), p the leadscrew pitch (i.e., 0.2 mm), and *mOffset* specifies how far the needle wire(s) is moved.

```
//This function is responsible for making the selected motor move. The function receives
information
// about motor, speed (i.e. delay) and protrusion offset as an input.

void moveMotor (unsigned char motorMask, int mDelay, float mOffset)
{
    int numSteps = 5*20*mOffset; // b/c 5 revolutions equal 1mm travel distance and 20 excitations
    are required for one rev. in full step mode.

    for(int counter = 0; counter <= numSteps-1; counter++)
    {
        STEP.COMBINED.MOTORS = motorMask;
        delayMicroseconds(mDelay);
        STEP.COMBINED.MOTORS = ~STEP.COMBINED.MOTORS & motorMask;
        delayMicroseconds(mDelay);
    }
}
```


C

EXPERIMENTS

C.1. EXPERIMENT 1

Table C.1 shows the order in which the experimental trials of Experiment 1 were performed.

Table C.1: Trials of Experiment 1.

Trial No.	Actuation Pattern	Gelatin Weight [g]	Date (DD-MM-YYYY)
1	single	184	16-02-2016
2	paired	187	16-02-2016
3	single	186	16-02-2016
4	single	187	16-02-2016
5	paired	189	16-02-2016
6	single	183	16-02-2016
7	paired	187	16-02-2016
8	paired	187	16-02-2016
9	paired	184	16-02-2016
10	single	188	16-02-2016
11	paired	188	16-02-2016
12	single	186	16-02-2016

C.2. EXPERIMENT 2

Table C.2 shows the order in which the experimental trials of Experiment 2 were performed and which trials were tested on what day. The ten conditions represent ten different combinations of settings for the bevel offset, the dynamic offset and the steering direction as specified in Table I in the scientific paper.

Table C.2: Trials of Experiment 2.

Trial No.	Condition No.	Gelatin Weight [g]	Date (DD-MM-YYYY)
1	5	187	22-02-2016
2	10	183	17-02-2016
3	8	187	17-02-2016
4	6	188	22-02-2016
5	7	185	18-02-2016
6	9	189	18-02-2016
7	5	187	22-02-2016
8	8	188	18-02-2016
9	1	189	18-02-2016
10	8	188	18-02-2016
11	10	189	18-02-2016
12	4	188	22-02-2016
13	1	186	23-02-2016
14	1	184	23-02-2016
15	6	186	23-02-2016
16	7	187	23-02-2016
17	3	186	23-02-2016
18	6	185	23-02-2016
19	9	187	23-02-2016
20	5	186	23-02-2016
21	9	186	23-02-2016
22	8	187	23-02-2016
23	6	187	24-02-2016
24	9	187	24-02-2016
25	10	189	24-02-2016
26	2	188	24-02-2016
27	7	188	24-02-2016
28	2	186	25-02-2016
29	5	186	25-02-2016
30	4	189	25-02-2016
31	4	185	25-02-2016
32	6	187	25-02-2016
33	10	189	26-02-2016
34	1	188	26-02-2016
35	2	186	26-02-2016
36	7	187	26-02-2016
37	3	185	26-02-2016
38	3	186	26-02-2016
39	8	187	26-02-2016
40	5	188	26-02-2016
41	9	187	26-02-2016
42	1	184	26-02-2016
43	7	181	01-03-2016
44	2	188	01-03-2016
45	4	188	01-03-2016
46	3	188	01-03-2016
47	10	189	01-03-2016
48	4	185	01-03-2016
49	3	185	01-03-2016
50	2	186	01-03-2016

D

MATLAB Code

D.1. EXPERIMENT 1 (SLIP ANALYSIS)

This section contains the MATLAB code for the data analysis of Experiment 1. Running the analysis file (SlipAnalysis.mat) requires the file slipData.mat of which an electronic copy was submitted to the supervisors along with this report. The file MagInset.m was downloaded from the MathWorks website¹.

```
1
2 %%%%%%%%%%%%%%%%%%%%%%%%%%%%%%%%%%%%%%%%%%%%%%%%%%%%%%%%%%%%%%%%%%%%%%%%%
3 %MATLAB code for performing the slip analysis of Experiment 1
4 %Author:          Tim Pusch
5 %Last update:    03/05/2016
6 %%%%%%%%%%%%%%%%%%%%%%%%%%%%%%%%%%%%%%%%%%%%%%%%%%%%%%%%%%%%%%%%%%%%%%%%%
7
8 %% initialize
9 clear all
10 close all
11 clc
12
13 load 'slipData.mat'
14
15 %% constants / data processing
16
17 f = 5; %sampling rate [Hz]
18
19 cDist = 4; %theoretical travel distance per cycle [mm]
20 thDist = 120; %theoretical total travel distance for each experiment [mm]
21 vIns = 2; %pushing and pulling speed [mm/s]
22
23
24 %convert to seconds and zero starting point
25 for jj=1:length(allData)
26
27     Dat_sec{jj} = linspace(0, length(allData{jj})/f, length(allData{jj}));
28     Dat_zer{jj} = allData{jj}(:,3) - allData{jj}(1,3);
29
30     allData_pr{jj} = [Dat_sec{jj}', allData{jj}(:,2), Dat_zer{jj}];
31
32     trDist(jj) = Dat_zer{jj}(end);
33 end
34
35 travDist_mean1w = sum([trDist(1), trDist(3), trDist(4), trDist(6), trDist(12)])/5;
36 travDist_mean2w = sum([trDist(2), trDist(5), trDist(7), trDist(8), trDist(9), ...
37     trDist(11)])/6;
38
39 %% slip per cycle (with processed data, i.e. zeroed starting point and time x-axis)
40
```

¹<http://www.mathworks.com/matlabcentral/fileexchange/49055-maginet>

```

41 pk_thr = 1.7;
42 va_thr = 1;
43
44 for s=1:length(allData_pr)
45
46     i = 1;
47     m = 1;
48
49     if s==6
50         pk_thr = 1.5;
51     end
52
53     [pk,lc_pk] = findpeaks(allData_pr{s}(:,3),allData_pr{s}(:,1)); %find maxima
54     DataInv = 2*allData_pr{s}(1,3)-allData_pr{s}(:,3); %build inverse of data
55     [va,lc_va] = findpeaks(DataInv,allData_pr{s}(:,1)); %find minima
56
57     for ii=1:length(pk)-1
58
59         if ii < length(va)
60
61             pkDiff(ii) = abs(pk(ii)-pk(ii+1));
62             vaDiff(ii) = abs(va(ii)-va(ii+1));
63
64             if pkDiff(ii) > pk_thr
65                 mins_pk(i,:) = [pk(ii), lc_pk(ii)];
66                 maxs_pk(i,:) = [pk(ii+1), lc_pk(ii+1)];
67
68                 i=i+1;
69             end
70
71             if vaDiff(ii) > va_thr
72                 mins_va(m,:) = [va(ii), lc_va(ii)];
73                 maxs_va(m,:) = [va(ii+1), lc_va(ii+1)];
74
75                 m=m+1;
76             end
77
78         end
79
80     end
81
82
83
84     maxs_pks{s} = [allData_pr{s}(1,3),0; maxs_pk]; %add starting point as first maximum
85     mins_vas{s} = [mins_va(:,1)+2*(allData_pr{s}(1,3)-mins_va(:,1)), mins_va(:,2)]; ...
86         %project on real curve
87
88
89     for kk=1:length(maxs_pks{s})-1
90
91         protDist(kk) = abs(maxs_pks{s}(kk,1)-mins_vas{s}(kk,1));
92         retr(kk) = abs(maxs_pks{s}(kk+1,1)-mins_vas{s}(kk,1));
93         forwDist(kk) = abs(maxs_pks{s}(kk+1,1)-maxs_pks{s}(kk,1));
94
95         slipCycl(kk) = forwDist(kk)/cDist;
96         slipRetr(kk) = retr(kk)/cDist;
97
98     end
99
100     protDists{s} = protDist;
101     slipRetrs{s} = slipRetr;
102     forwDists{s} = forwDist;
103     slipCycls{s} = slipCycl;
104     retrs{s} = retr;
105
106
107 end
108
109 %grouped slip (measured/theoretical):
110

```



```

111 eff_1w = [slipCycles{1}', slipCycles{3}', slipCycles{4}', slipCycles{6}', ...
           slipCycles{12}']; %without exp. 10
112 mEff_1w = mean(eff_1w,2);
113
114 eff_2w = [slipCycles{2}', slipCycles{5}', slipCycles{7}', slipCycles{8}', slipCycles{9}',...
           slipCycles{11}']; %without exp. 10
115 mEff_2w = mean(eff_2w,2);
116
117
118 %slip (1 - measured/theoretical):
119 slip_1w = 1 - eff_1w;
120 mSlip_1w = mean(slip_1w, 2);
121 slip_2w = 1 - eff_2w;
122 mSlip_2w = mean(slip_2w, 2);
123
124
125 %forward motion in retraction (pulling) step:
126 mRetr_1w = mean([retrs{1}', retrs{3}', retrs{4}', retrs{6}', retrs{12}'], 2);
127 mRetr_2w = mean([retrs{2}', retrs{5}', retrs{7}', retrs{8}', retrs{9}', retrs{11}'], 2);
128
129
130 %backward motion in pushing step:
131 mProtDist_1w = mean([protDists{1}', protDists{3}', protDists{4}', protDists{6}', ...
                     protDists{12}'], 2);
132 mProtDist_2w = mean([protDists{2}', protDists{5}', protDists{7}', protDists{8}',...
                     protDists{9}', protDists{11}'], 2);
133
134
135
136 %% Insertion speed
137
138 for v=1:length(maxs_pks)
139
140     DistPerTime_all(v,:) = maxs_pks{v}(2,:) - maxs_pks{v}(end,:);
141     InSpeed_all(v) = DistPerTime_all(v,1)/DistPerTime_all(v,2);
142
143 end
144
145 InSpeed_sing = InSpeed_all([1,3,4,6,12]);
146 InSpeed_pair = InSpeed_all([2,5,7,8,9,11]);
147
148 InSpeedMean_sing = mean(InSpeed_sing);
149 InSpeedMean_pair = mean(InSpeed_pair);
150
151
152 %% plot results
153
154 %Plots distance that the cart is pulled towards needle base per cycle
155 figure
156 for a=1:length(allData_pr)
157     if a==1 || a==3 || a==4 || a==6 || a==12 %single actuation
158         R1(a) = plot(retrs{a}, 'k-.');
159         hold on
160     end
161 end
162 hold on
163 MR1 = plot(mRetr_1w, 'k-', 'LineWidth', 2);
164
165 hold on
166 for aa=1:length(allData_pr)
167     if aa==2 || aa==5 || aa==7 || aa==8 || aa==9 || aa==11 %paired actuation
168         R2(aa) = plot(retrs{aa}, 'r-.');
169         hold on
170     end
171 end
172 hold on
173 MR2 = plot(mRetr_2w, 'r-', 'LineWidth', 2);
174 title('Distance cart travels in pulling step')
175 RetrLeg1 = sprintf('Data sets single actuation');
176 RetrLeg2 = sprintf('Data sets paired actuation');
177 RetrLeg3 = sprintf('Mean single actuation');
178 RetrLeg4 = sprintf('Mean paired actuation');
179 legend([R1(1) R2(2) MR1 MR2], RetrLeg1, RetrLeg2, RetrLeg3, RetrLeg4)

```

```

180 ylim([1.5 4])
181 xlim([1 30])
182 xlabel('Number of cycle', 'FontSize', 12)
183 ylabel('Measured distance [mm]', 'FontSize', 12)
184
185
186
187 %Plots distance that the cart is pushed away from needle base per cycle
188 figure
189 for b=1:length(allData_pr)
190     if b==1 || b==3 || b==4 || b==6 || b==12 %single actuation
191         P1(b) = plot(protDists{b}, 'k-.');
192         hold on
193     end
194 end
195 hold on
196 MP1 = plot(mProtDist_1w, 'k-', 'LineWidth', 2);
197
198 hold on
199 for bb=1:length(allData_pr)
200     if bb==2 || bb==5 || bb==7 || bb==8 || bb==9 || bb==11 %single actuation
201         P2(bb) = plot(protDists{bb}, 'r-.');
202         hold on
203     end
204 end
205 hold on
206 MP2 = plot(mProtDist_2w, 'r-', 'LineWidth', 2);
207 title('Distance cart is pushed back')
208 ProtLeg1 = sprintf('Data sets single actuation');
209 ProtLeg2 = sprintf('Data sets paired actuation');
210 ProtLeg3 = sprintf('Mean single actuation');
211 ProtLeg4 = sprintf('Mean paired actuation');
212 legend([P1(1) P2(2) MP1 MP2], ProtLeg1, ProtLeg2, ProtLeg3, ProtLeg4)
213 ylim([0 2])
214 xlim([1 30])
215 xlabel('Number of cycle', 'FontSize', 12)
216 ylabel('Measured distance [mm]', 'FontSize', 12)
217
218
219
220 %Plots all trial data of the experiment
221 figure
222 for pp=1:length(allData_pr)
223     if pp ≤ 9 || pp>10 %don't plot exp. 10
224         plot(allData_pr{pp}(:,1), allData_pr{pp}(:,3))
225         ylim([-5 120])
226         hold on
227     end
228 end
229 hold on
230 t1 = plot([0 450],[travDist_mean1w travDist_mean1w],'k--', 'LineWidth', 2);
231 hold on
232 t2 = plot([0 450],[travDist_mean2w travDist_mean2w],'k-.', 'LineWidth', 2);
233 xlabel('Time [s]', 'FontSize', 14)
234 ylabel('Measured travelled distance [mm]', 'FontSize', 14)
235 title('Straight path experiments - All experimental trials', 'FontSize', 16)
236 legend([t1, t2], 'Mean travelled distance one-wire actuation', 'Mean travelled ...
    distance two-wire actuation')
237
238
239
240 %Plots the example of a trial used in the scientific paper
241 num = 1; %number of experimental trial
242 fig1 = figure;
243 set(fig1, 'Position', [1000 300 700 500])
244 plot(allData_pr{num}(:,1), allData_pr{num}(:,3), 'LineWidth', 1.5)
245 hold on
246 plot(maxs_pks{num}(:,2),maxs_pks{num}(:,1),'ro', 'LineWidth', 0.5)
247 % hold on
248 % plot(mins_vas{num}(:,2),mins_vas{num}(:,1),'kx', 'LineWidth', 0.5)
249 xlabel('Time [s]', 'FontSize', 14)

```

```

250 ylabel('Measured traveled distance [mm]', 'FontSize', 14)
251 xlim([0 allData_pr{num}(end,1)+20])
252 ylim([-10 120])
253 title3=sprintf('Experimental trial No. %d', num);
254 % title(title3, 'FontSize', 16)
255 set(gca, 'FontSize', 12)
256 %MagInset
257 MagInset(fig1, -1, [213 235 46 51], [50 180 60 100], {'NE','NE';'SW','SW'}); %adjust ...
    to fit needs
258 grid on
259 % txt1 = 'v_1';
260 txt2 = 'p_n';
261 txt3 = 'p_{n+1}';
262 % text(mins_vas{num}(1,2)+2,mins_vas{num}(1,1)-0.2,txt1, 'FontWeight', 'bold', ...
    'FontSize', 12)
263 text(maxs_pks{num}(16,2),maxs_pks{num}(16,1)+0.8,txt2, 'FontWeight', 'bold', ...
    'FontSize', 12)
264 text(maxs_pks{num}(17,2)-6,maxs_pks{num}(17,1),txt3, 'FontWeight', 'bold', ...
    'FontSize', 12)
265
266
267
268 %% efficiency plots (eff. = traveled distance / theor. travel distance)
269
270 %Single (one-wire) actuation
271 figure
272 for pp=1:length(eff_1w(1,:))
273     plot(eff_1w(:,pp))
274     hold on
275 end
276 plot(mEff_1w, 'LineWidth', 3)
277 xlabel('Number of cycle', 'FontSize', 14)
278 ylabel('Travel efficiency', 'FontSize', 14)
279 title('One-wire actuation', 'FontSize', 18)
280 legend('Exp. 1', 'Exp. 3', 'Exp. 4', 'Exp. 6', 'Exp. 12', 'Mean')
281
282 %Double (two-wire) actuation
283 figure
284 for tt=1:length(eff_2w(1,:))
285     plot(eff_2w(:,tt))
286     hold on
287 end
288 plot(mEff_2w, 'LineWidth', 3)
289 xlabel('Number of cycle', 'FontSize', 14)
290 ylabel('Travel efficiency', 'FontSize', 14)
291 title('Two-wire actuation', 'FontSize', 18)
292 legend('Exp. 2', 'Exp. 5', 'Exp. 7', 'Exp. 8', 'Exp. 9', 'Exp. 11', 'Mean')
293
294 %Combined means
295 figure
296 plot(mEff_1w, 'LineWidth', 3)
297 hold on
298 plot(mEff_2w, 'LineWidth', 3)
299 hold on
300 plot([9 9], [0.8 0.85], 'k-')
301 leg1 = sprintf('Mean travelled distance [mm]: %10.1f\n',...
    round(sum(mEff_1w(1:9).*4),1));
302 plot([9 9], [0.66 0.71], 'k-')
303 leg2 = sprintf('Mean travelled distance [mm]: %10.1f\n',...
    round(sum(mEff_2w(1:9).*4),1));
304
305
306 grid on
307 xlabel('Number of cycle', 'FontSize', 14)
308 ylabel('Travel efficiency', 'FontSize', 14)
309 legend('one-wire actuation', 'two-wire actuation', leg1, leg2)
310 title('Means of travel efficiency', 'FontSize', 18)
311
312
313 %% Slip plots (slip = 1 - eff.)
314
315 %Single (one-wire) actuation
316 figure

```

```

317 for pp=1:length(slip_1w(1,:))
318     plot(slip_1w(:,pp), 'b-.')
319     hold on
320 end
321 plot(mSlip_1w, 'b-', 'LineWidth', 3)
322 xlabel('Number of cycle', 'FontSize', 14)
323 ylabel('Slip ratio', 'FontSize', 14)
324 title('One-wire actuation', 'FontSize', 18)
325 legend('Exp. 1', 'Exp. 3', 'Exp. 4', 'Exp. 6', 'Exp. 12', 'Mean')
326
327 %Double (two-wire) actuation
328 figure
329 for tt=1:length(slip_2w(1,:))
330     plot(slip_2w(:,tt), 'r-.')
331     hold on
332 end
333 plot(mSlip_2w, 'r-', 'LineWidth', 3)
334 xlabel('Number of cycle', 'FontSize', 14)
335 ylabel('Slip ratio', 'FontSize', 14)
336 title('Two-wire actuation', 'FontSize', 18)
337 legend('Exp. 2', 'Exp. 5', 'Exp. 7', 'Exp. 8', 'Exp. 9', 'Exp. 11', 'Mean')
338
339 %Combined means
340 figure
341 plot(mSlip_1w, 'LineWidth', 3)
342 hold on
343 plot(mSlip_2w, 'LineWidth', 3)
344 hold on
345 grid on
346 xlabel('Number of cycle', 'FontSize', 14)
347 ylabel('Mean slip ratio', 'FontSize', 14)
348 legend('one-wire actuation (n = 5)', 'two-wire actuation (n = 6)')
349 title('Means of slip ratio', 'FontSize', 18)
350
351
352 %Combined means and individual trials
353 figure
354 for pp=1:length(slip_1w(1,:))
355     MS1(pp) = plot(slip_1w(:,pp), 'k:');
356     hold on
357     MS2(pp) = plot(slip_2w(:,pp), 'r--');
358     hold on
359 end
360 M1 = plot(mSlip_1w, 'k-.', 'LineWidth', 3);
361 hold on
362 M2 = plot(mSlip_2w, 'r-', 'LineWidth', 3);
363 xlabel('Number of cycle', 'FontSize', 12)
364 ylabel('Slip ratio', 'FontSize', 12)
365 legM1 = sprintf('Mean of single actuation trials (n = 5)');
366 legM2 = sprintf('Mean of paired actuation trials (n = 6)');
367 legMS1 = sprintf('Single actuation trials');
368 legMS2 = sprintf('Paired actuation trials');
369 legend([MS1(1) MS2(1) M1 M2], legMS1, legMS2, legM1, legM2)
370 set(gca, 'FontSize', 12)
371 grid on
372 xlim([1 30])
373
374
375 %% Plots of raw data of experimental trials
376
377 %Single actuation
378 figure
379 plot(allData{1}(:,1), allData{1}(:,3))
380 hold on
381 plot(allData{3}(:,1), allData{3}(:,3))
382 hold on
383 plot(allData{4}(:,1), allData{4}(:,3))
384 hold on
385 plot(allData{6}(:,1), allData{6}(:,3))
386 hold on
387 plot(allData{10}(:,1), allData{10}(:,3))

```

```

388 hold on
389 plot(allData{12}(:,1), allData{12}(:,3))
390 legend('Test No. 1', 'Test No. 3', 'Test No. 4', 'Test No. 6',...
391        'Test No. 10', 'Test No. 12')
392
393 %Double actuation
394 figure
395 plot(allData{2}(:,1), allData{2}(:,3))
396 hold on
397 plot(allData{5}(:,1), allData{5}(:,3))
398 hold on
399 plot(allData{7}(:,1), allData{7}(:,3))
400 hold on
401 plot(allData{8}(:,1), allData{8}(:,3))
402 hold on
403 plot(allData{9}(:,1), allData{9}(:,3))
404 hold on
405 plot(allData{11}(:,1), allData{11}(:,3))
406 legend('Test No. 2', 'Test No. 5', 'Test No. 7', 'Test No. 8',...
407        'Test No. 9', 'Test No. 11')

```

D.2. EXPERIMENT 2 (STEERING ANALYSIS)

This section contains the MATLAB code for the analysis of Experiment 2. The code requires the file `images.mat` containing the pictures taken during the experiment. An electronic copy of this file was submitted to the supervisors along with this report. The function `circfit.m` was downloaded from the MathWorks website². In order to perform the analysis, the `.mat` files should be run in the following order:

1. Run `cropImages.mat` to crop the pictures.
2. Run `ImProcessing.mat` to perform the image processing.
3. Run `SteeringAnalysis.mat` to perform the final analysis.

THE CROPIMAGES.MAT FILE

```

1
2 %%%%%%%%%%%%%%%%%%%%%%%%%%%%%%%%%%%%%%%%%%%%%%%%%%%%%%%%%%%%%%%%%%%%%%%%%
3 %MATLAB code for cropping the images to be used in the steering analysis
4 %of Experiment 2.
5 %Author:      Tim Pusch
6 %Last update: 29/04/2016
7 %%%%%%%%%%%%%%%%%%%%%%%%%%%%%%%%%%%%%%%%%%%%%%%%%%%%%%%%%%%%%%%%%%%%%%%%%
8
9 clear all
10 close all
11 clc
12
13 load images.mat; %load workspace with pictures from experiments
14
15
16 %% Group images
17 %create groups for each condition containing the five experiments.
18
19 cond01 = {images{9}, images{13}, images{14}, images{34}, images{42}};
20 cond02 = {images{26}, images{28}, images{35}, images{44}, images{50}};
21 cond03 = {images{17}, images{37}, images{38}, images{46}, images{49}};
22 cond04 = {images{12}, images{30}, images{31}, images{45}, images{48}};
23 cond05 = {images{1}, images{7}, images{20}, images{29}, images{40}};
24 cond06 = {images{4}, images{15}, images{18}, images{23}, images{32}};
25 cond07 = {images{5}, images{16}, images{27}, images{36}, images{43}};
26 cond08 = {images{3}, images{8}, images{10}, images{22}, images{39}};
27 cond09 = {images{6}, images{19}, images{21}, images{24}, images{41}};

```

²<http://www.mathworks.com/matlabcentral/fileexchange/5557-circle-fit/content/circfit.m>

```

28 cond10 = {images{2}, images{11}, images{25}, images{33}, images{47}};
29
30 conds = {cond01, cond02, cond03, cond04, cond05, cond06, cond07, cond08, cond09, cond10};
31
32 %% crop images
33
34 for i=1:length(conds)
35     for j=1:length(conds{i})
36         curCond = conds{i};
37         cropped = imcrop(curCond{j});
38         CRcond{j} = cropped;
39     end
40     CRconds{i} = CRcond;
41 end
42
43 save('croppedIm2.mat', 'CRconds', '-v7.3');

```

THE IMPROCESSING.MAT FILE

```

1
2 %%%%%%%%%%%%%%%%%%%%%%%%%%%%%%%%%%%%%%%%%%%%%%%%%%%%%%%%%%%%%%%%%%%%%%%%%
3 %MATLAB code for performing the image processing for the steering analysis
4 %of Experiment 2.
5 %Author:          Tim Pusch
6 %Last update:    29/04/2016
7 %%%%%%%%%%%%%%%%%%%%%%%%%%%%%%%%%%%%%%%%%%%%%%%%%%%%%%%%%%%%%%%%%%%%%%%%%
8
9 clear all
10 close all
11 clc
12
13 load croppedIm2.mat; %load workspace with pictures from experiments
14
15 %% Image processing and scaling factor
16
17 for jj=1:length(CRconds)
18
19     CRcond = CRconds{jj};
20
21     for m=1:length(CRcond)
22
23         imAdj = imadjust(CRcond{m}, stretchlim(CRcond{m}), [0.2 0.8]); %contrast stretch
24         imBW = im2bw(imAdj, 0.2); %convert to BW and create complementary images:
25         imBW = bwmorph(imBW, 'majority', 50); %get rid of noise
26         imBW = bwmorph(imBW, 'dilate', 2); %get rid of noise
27         imBWInv = imcomplement(imBW); %build complementary image
28         skel = bwmorph(imBWInv, 'skel', Inf); %create skeleton
29         spur = bwmorph(skel, 'spur', 50); %trim branches
30         clean = bwmorph(spur, 'clean'); %remove isolated pixels
31         imProc{m} = clean; %store in variable
32
33         %scaling factor (pix to mm)
34         imSize = size(CRcond{m}); %find image size in pixels
35         scF{m} = 120/imSize(2); %convert to mm based on grid information
36
37     end
38
39     imSProc{jj} = imProc; %all processed images
40     scFs{jj} = scF; %all scaling factors
41     jj
42
43 end
44
45 save('procedIm2.mat', '-v7.3');

```

THE STEERINGANALYSIS.MAT FILE

```

1
2  %%%%%%%%%%%%%%%%%%%%%%%%%%%%%%%%%%%%%%%%%%%%%%%%%%%%%%%%%%%%%%%%%%%%%%%%%
3  %MATLAB code for performing the steering analysis of Experiment 2
4  %Author:      Tim Pusch
5  %Last update: 03/05/2016
6  %%%%%%%%%%%%%%%%%%%%%%%%%%%%%%%%%%%%%%%%%%%%%%%%%%%%%%%%%%%%%%%%%%%%%%%%%
7
8  clear all
9  close all
10 clc
11
12 load 'procedIm2.mat'; %load workspace with processed pictures from experiments
13
14 %% Plot cropped images
15
16 for ii=1:length(CRconds)
17
18     CRcond = CRconds{ii};
19
20     figure
21     subplot(511)
22     imshow(CRcond{1})
23     subplot(512)
24     imshow(CRcond{2})
25     subplot(513)
26     imshow(CRcond{3})
27     subplot(514)
28     imshow(CRcond{4})
29     subplot(515)
30     imshow(CRcond{5})
31
32     str=sprintf('Condition %d', ii);
33     subplot(str)
34
35 end
36
37 %% convert binary to double
38
39 for kk=1:length(imSProc)
40
41     imProc = imSProc{kk};
42
43     for n=1:length(imProc)
44
45         [a, b] = find(imProc{n});
46         A{n} = a;
47         B{n} = b;
48         C{n} = [B{n}, -A{n}];
49
50     end
51
52     As{kk} = A;
53     Bs{kk} = B;
54     Cs{kk} = C;
55
56 end
57
58 %Plot results
59 for ll=1:length(As)
60
61     A = As{ll};
62     B = Bs{ll};
63
64     %
65     figure
66     %
67     subplot(511)
68     %
69     plot(B{1}, -A{1}, '.')
70     %
71     axis([500 3500 -1000 -200])

```

```

69 % subplot(512)
70 % plot(B{2}, -A{2}, '.')
71 % axis([500 3500 -1000 -200])
72 % subplot(513)
73 % plot(B{3}, -A{3}, '.')
74 % axis([500 3500 -1000 -200])
75 % subplot(514)
76 % plot(B{4}, -A{4}, '.')
77 % axis([500 3500 -1000 -200])
78 % subplot(515)
79 % plot(B{5}, -A{5}, '.')
80 % axis([500 3500 -1000 -200])
81
82 figure
83 plot(B{1}, -A{1}, '.')
84 hold on
85 plot(B{2}, -A{2}, '.')
86 hold on
87 plot(B{3}, -A{3}, '.')
88 hold on
89 plot(B{4}, -A{4}, '.')
90 hold on
91 plot(B{5}, -A{5}, '.')
92 % axis([750 3500 -600 -200])
93
94 end
95
96 %% manually remove noise
97
98 %Remove noise pixels from trial 3 of condition 1:
99 Crem1 = Cs{1};
100 Crem1{3}(1:7,:) = [];
101 Cs{1} = Crem1;
102
103 %Remove noise pixels from trial 1 of condition 2:
104 Crem2 = Cs{2};
105 Crem2{1}(1:49,:) = [];
106 Cs{2} = Crem2;
107
108
109 %% Fit radius
110
111 for qq=1:length(Cs)
112     C = Cs{qq};
113     scF = scFs{qq};
114     for o=1:length(C)
115         [xfit,yfit,rfit] = circfit(C{o}(:,1),C{o}(:,2));
116
117         ang=0:0.001:2*pi;
118         xp=rfit*cos(ang);
119         yp=rfit*sin(ang);
120
121         Xfit(o) = xfit;
122         XfitSc(o) = xfit*scF(o);
123         Yfit(o) = yfit;
124         YfitSc(o) = yfit*scF(o);
125         Rfit(o) = rfit;
126         RfitSc(o) = rfit*scF(o);
127         Xp{o} = xp;
128         Yp{o} = yp;
129     end
130
131 Xfits{qq} = Xfit;
132 XfitsSc{qq} = XfitSc;
133 Yfits{qq} = Yfit;
134 YfitsSc{qq} = YfitSc;

```



```

140     Rfits{qq} = Rfit;
141     RfitsSc{qq} = RfitSc;
142     Xps{qq} = Xp;
143     Yps{qq} = Yp;
144
145 end
146
147
148 %Plot results
149 for pp=1:length(Cs)
150
151     C = Cs{pp};
152     Xfit = Xfits{pp};
153     Yfit = Yfits{pp};
154     Rfit = Rfits{pp};
155     Xp = Xps{pp};
156     Yp = Yps{pp};
157
158     figure
159     subplot(511)
160     plot(C{1}(:,1), C{1}(:,2), 'LineWidth', 2)
161     hold on
162     plot(Xfit(1)+Xp{1}, Yfit(1)+Yp{1}, 'r')
163     axis([400 3500 -1000 -200])
164     subplot(512)
165     plot(C{2}(:,1), C{2}(:,2), 'LineWidth', 2)
166     hold on
167     plot(Xfit(2)+Xp{2}, Yfit(2)+Yp{2}, 'r')
168     axis([400 3500 -1000 -200])
169     subplot(513)
170     plot(C{3}(:,1), C{3}(:,2), 'LineWidth', 2)
171     hold on
172     plot(Xfit(3)+Xp{3}, Yfit(3)+Yp{3}, 'r')
173     axis([400 3500 -1000 -200])
174     subplot(514)
175     plot(C{4}(:,1), C{4}(:,2), 'LineWidth', 2)
176     hold on
177     plot(Xfit(4)+Xp{4}, Yfit(4)+Yp{4}, 'r')
178     axis([400 3500 -1000 -200])
179     subplot(515)
180     plot(C{5}(:,1), C{5}(:,2), 'LineWidth', 2)
181     hold on
182     plot(Xfit(5)+Xp{5}, Yfit(5)+Yp{5}, 'r')
183     axis([400 3500 -1000 -200])
184
185 end
186
187
188 %% Post-processing (in [1/cm])
189
190 %curvature is set to 0 if needle steers in wrong direction
191
192 %condition 3:
193 curCond3_1 = 0;
194 corrCurCond3 = [curCond3_1, 10./RfitsSc{3}(2), 10./RfitsSc{3}(3), 10./RfitsSc{3}(4), ...
195     10./RfitsSc{3}(5),];
196
197 %condition 5:
198 curCond5_2 = 0;
199 corrCurCond5 = [10./RfitsSc{5}(1), curCond5_2, 10./RfitsSc{5}(3), 10./RfitsSc{5}(4), ...
200     10./RfitsSc{5}(5),];
201
202 %condition 7:
203 curCond7_2 = 0;
204 curCond7_3 = 0;
205 curCond7_4 = 0;
206 curCond7_5 = 0;
207 corrCurCond7 = [10./RfitsSc{7}(1), curCond7_2, curCond7_3, curCond7_4, curCond7_5];
208
209 %condition 9:
210 curCond9_2 = 0;

```

```

209 curCond9_3 = 0;
210 curCond9_4 = 0;
211 curCond9_5 = 0;
212 corrCurCond9 = [10./RfitsSc{9}(1), curCond9_2, curCond9_3, curCond9_4, curCond9_5];
213
214
215 %Post-processing for results plots [1/cm]
216 condKs = [(10./RfitsSc{1})', (10./RfitsSc{2})', (10./RfitsSc{3})', (10./RfitsSc{4})',...
217           (10./RfitsSc{5})', (10./RfitsSc{6})', (10./RfitsSc{7})', (10./RfitsSc{8})',...
218           (10./RfitsSc{9})', (10./RfitsSc{10})'];
219
220 corrCondKs = [(10./RfitsSc{1})', (10./RfitsSc{2})', corrCurCond3', (10./RfitsSc{4})',...
221              corrCurCond5', (10./RfitsSc{6})', corrCurCond7', (10./RfitsSc{8})',...
222              corrCurCond9', (10./RfitsSc{10})'];
223
224 condNames = ['C1', 'C2', 'C3', 'C4', 'C5', 'C6', 'C7', 'C8', 'C9', 'C10'];
225
226 %% plots (with curvature correction)
227
228 %all conditions:
229 figure
230 boxplot(corrCondKs, {'C1', 'C2', 'C3', 'C4', 'C5', 'C6', 'C7', 'C8', 'C9', 'C10'})
231 ylabel('Curvature [1/cm]', 'FontSize', 14)
232 xlabel('Conditions', 'FontSize', 14)
233 title('All conditions', 'FontSize', 18)
234
235 %constant BO conditions:
236 figure
237 boxplot([corrCondKs(:,1), corrCondKs(:,7), corrCondKs(:,9), corrCondKs(:,2), ...
238         corrCondKs(:,8), corrCondKs(:,10)], {'2.0 ', '4.0 ',...
239         ' 6.0 ', ' 2.0', ' 4.0', ' 6.0'})
240 hold on
241 plot([3.5, 3.5],[0, 0.025], 'k-.')
242 text(2, 0.0225, 'Left', 'FontSize', 11, 'HorizontalAlignment', 'center')
243 text(5, 0.0225, 'Right', 'FontSize', 11, 'HorizontalAlignment', 'center')
244 ylabel('Curvature [1/cm]', 'FontSize', 12)
245 xlabel('Dynamic Offset [mm]', 'FontSize', 12)
246 % title('Constant bevel offset (BO): 3.6mm', 'FontSize', 18)
247 ylim([0 0.025])
248 set(gca, 'YTickLabel', num2str(get(gca, 'YTick').'))
249
250 %constant DO conditions:
251 figure
252 boxplot([corrCondKs(:,5), corrCondKs(:,3), corrCondKs(:,7), corrCondKs(:,6),...
253         corrCondKs(:,4), corrCondKs(:,8)], {'0.9 ', '1.8 ',...
254         '3.6 ', ' 0.9', ' 1.8', ' 3.6'})
255 hold on
256 plot([3.5, 3.5],[0, 0.025], 'k-.')
257 text(2, 0.0225, 'Left', 'FontSize', 11, 'HorizontalAlignment', 'center')
258 text(5, 0.0225, 'Right', 'FontSize', 11, 'HorizontalAlignment', 'center')
259 ylabel('Curvature [1/cm]', 'FontSize', 12)
260 xlabel('Bevel Offset [mm]', 'FontSize', 12)
261 % title('Constant cycle offset (CO): 4.0mm', 'FontSize', 18)
262 ylim([0 0.025])
263 set(gca, 'YTickLabel', num2str(get(gca, 'YTick').'))
264
265 %Test - Boxplots with overlaid raw data (constant BO):
266 figure
267 boxplot([corrCondKs(:,1), corrCondKs(:,7), corrCondKs(:,9), corrCondKs(:,2), ...
268         corrCondKs(:,8), corrCondKs(:,10)], {'Cond. 1', 'Cond. 7',...
269         'Cond. 9', 'Cond. 2', 'Cond. 8', 'Cond. 10'})
270 hold on
271 plot([1.35, 2.35, 3.35, 4.35, 5.35, 6.35], [corrCondKs(:,1), corrCondKs(:,7), ...
272         corrCondKs(:,9), corrCondKs(:,2), ...
273         corrCondKs(:,8), corrCondKs(:,10)], 'o', ...
274         'MarkerEdgeColor', 'k', 'MarkerFaceColor', [1 0.5 0.5], 'MarkerSize', 5)
275 ylabel('Curvature [1/cm]', 'FontSize', 12)
276 xlabel('Conditions', 'FontSize', 12)
277 % title('Constant bevel offset (BO): 3.6mm', 'FontSize', 18)
278 ylim([0 0.025])
279 set(gca, 'YTickLabel', num2str(get(gca, 'YTick').'))

```

```

278
279
280 %% plots (not corrected for wrong steering direction)
281
282 %all conditions:
283 figure
284 boxplot(condKs, {'C1', 'C2', 'C3', 'C4', 'C5', 'C6', 'C7', 'C8', 'C9', 'C10'})
285 ylabel('Curvature [1/cm]', 'FontSize', 14)
286 xlabel('Conditions', 'FontSize', 14)
287 title('All conditions', 'FontSize', 18)
288
289 %constant BO conditions:
290 figure
291 boxplot([condKs(:,1), condKs(:,7), condKs(:,9), condKs(:,2), condKs(:,8), ...
292         condKs(:,10)],...
293         {'C1-L (CO: 2mm)', 'C7-L (CO: 4mm)', 'C9-L (CO: 6mm)', 'C2-R (CO: 2mm)', 'C8-R ...
294         (CO: 4mm)',...
295         'C10-R (CO: 6mm)'}])
296 ylabel('Curvature [1/cm]', 'FontSize', 14)
297 xlabel('Conditions', 'FontSize', 14)
298 title('Constant bevel offset (BO): 3.6mm', 'FontSize', 18)
299
300 %constant DO conditions:
301 figure
302 boxplot([condKs(:,5), condKs(:,3), condKs(:,7), condKs(:,6), condKs(:,4), ...
303         condKs(:,8)],...
304         {'C5-L (BO: 0.9mm)', 'C3-L (BO: 1.8mm)', 'C7-L (BO: 3.6mm)', 'C6-R (BO: 0.9mm)', ...
305         'C4-R (BO: 1.8mm)',...
306         'C8-R (BO: 3.6mm)'}])
307 ylabel('Curvature [1/cm]', 'FontSize', 14)
308 xlabel('Conditions', 'FontSize', 14)
309 title('Constant dynamic offset (DO): 4.0mm', 'FontSize', 18)
310
311 %% plot showing the data analysis steps
312
313 datAnCNum = 8; %Cond. 8
314 datAnTNum = 4; %Trial No. 4
315
316 DatAn_A = As{datAnCNum};
317 DatAn_B = Bs{datAnCNum};
318 DatAnXfit = Xfits{datAnCNum};
319 DatAnYfit = Yfits{datAnCNum};
320 DatAnRfit = Rfits{datAnCNum};
321 DatAnXp = Xps{datAnCNum};
322 DatAnYp = Yps{datAnCNum};
323 DatAnCRcond = CRconds{datAnCNum};
324
325 figure
326 subplot(211)
327 imshow(DatAnCRcond{datAnTNum})
328
329 subplot(212)
330 plot([-120 0], [0 0], 'k--', 'LineWidth', 0.25)
331 hold on
332 PL1 = plot(DatAn_B{datAnTNum}*scFs{datAnCNum}(datAnTNum)-120,...
333         -DatAn_A{datAnTNum}*scFs{datAnCNum}(datAnTNum)+20, 'k.', 'LineWidth', 4);
334 hold on
335 PL2 = plot((DatAnXfit(datAnTNum)+DatAnXp{datAnTNum})*scFs{datAnCNum}(datAnTNum)-120,...
336         (DatAnYfit(datAnTNum)+DatAnYp{datAnTNum})*scFs{datAnCNum}(datAnTNum)+20, 'r', ...
337         'LineWidth', 0.5);
338 axis([-120 0 -20 20])
339 set(gca, 'XAxisLocation', 'bottom', 'YAxisLocation', 'right');
340 set(gca, 'FontSize', 10)
341 xlabel('Length of cropped image [mm]')
342 ylabel('Width of cropped image [mm]')
343 legend([PL1 PL2], 'Extracted needle points', 'Circle fit: \kappa = 0.0152 1/cm')

```